UNIVERSITY OF CALIFORNIA, SAN DIEGO

The Role of Feedback in Signaling Dynamics

A dissertation submitted in partial satisfaction of the
requirements for the degree Doctor of Philosophy

in

Bioengineering

by

Diane Marie Longo

Committee in charge:

Jeff Hasty, Chair
Steve Briggs
Shu Chien
Alex Hoffmann
Amy Sung
Lev Tsimring

2009

The dissertation of Diane Marie Longo is approved, and it is acceptable in quality and form for publication on microfilm and electronically:

_____

_____

_____

_____

_____

_____

Chair

University of California, San Diego

2009

DEDICATION

To my parents

TABLE OF CONTENTS

Signature Page iii

Dedication iv

Table of Contents v

List of Abbreviations vii

List of Figures ix

List of Tables xi

Acknowledgements xii

Vita xiii

Abstract of the Dissertation xiv

Chapter 1 Introduction 1

1.1 Systems biology approach 1

1.2 Synthetic gene networks 3

1.3 Stochastic gene expression 6

1.4 Acknowledgements 9

Chapter 2 Coherent activation of a synthetic mammalian gene network 10

2.1 Introduction 10

2.2 Design and construction of a synthetic mammalian positive feedback network 12

2.3 Stochastic modeling of the mammalian synthetic network 13

2.4 Coherent activation with strong positive feedback 19

2.5 Naturally-occurring regulatory networks with positive feedback 23

2.6 Discussion 31

2.7 Materials and Methods 32

2.7.1 Network construction 32

2.7.2 Cell culture 32
2.7.3 Retroviral transductions 32
2.7.4 Flow cytometry 33
2.7.5 Modeling the synthetic network 33
2.8 Acknowledgements 34

Chapter 3 Dual delayed negative feedback model of NF-κB signaling 38
3.1 Introduction 38
3.2 NF-κB model with a single delayed negative feedback loop 41
3.3 Linear stability analysis of a single-feedback loop system 46
3.4 Damping of oscillations in a dual delayed feedback loop system 50
3.5 Fine temporal control with a dual feedback loop system 55
3.6 Additional role of negative feedback: robustness to fluctuations 63
3.7 Discussion 76
3.8 Materials and Methods 78
3.8.1 Cell culture experiments 78
3.8.2 Derivation of the deterministic model 79
3.8.3 Details of the linear stability analysis 82
3.8.4 Details of the BLASTP search for IκBα and IκBϵ homologs 83
3.9 Acknowledgements 83

Chapter 4 Concluding remarks 95

References 99

LIST OF ABBREVIATIONS

a.u. ..... arbitrary units
ATM ..... ataxia telangiectasia mutated
B. subtilis ..... *Bacillus subtilis*
BLAST ..... basic local alignment search tool
CFP ..... cyan fluorescent protein
CMV ..... cytomegalovirus
CO_2 ..... carbon dioxide
CV ..... coefficient of variation
DMEM ..... Dulbecco's Modification of Eagle's medium
DNA ..... deoxyribonucleic acid
dox ..... doxycycline
E. coli ..... *Escherichia coli*
EMSA ..... electrophoretic mobility shift assay
Eq. ..... equation
FACS ..... fluorescence activated cell sorting
FL ..... fluorescence
FSC ..... forward scatter
GFP ..... green fluorescent protein
hrs. ..... hours
IKK ..... IκB kinase
IκB ..... inhibitor of nuclear factor κB
MEF ..... murine embryonic fibroblast
μg ..... microgram
min ..... minutes
ml ..... milliliter
mRNA ..... messenger ribonucleic acid
NCBI ..... National Center for Biotechnology Information
NF-AT ..... nuclear factor of activated T-cells

NF-κB ..... nuclear factor κB
ODE ..... ordinary differential equation
PBS ..... phosphate buffered saline
PCR ..... polymerase chain reaction
r.h.s. ..... right hand side
RNA ..... ribonucleic acid
RPA ..... RNase protection assay
rtTA ..... tetracycline-regulated transactivator
S. cerevisiae ..... *Saccharomyces cerevisiae*
SNP ..... single nucleotide polymorphism
SSC ..... side scatter
tet ..... tetracycline
TNF ..... tumor necrosis factor
YFP ..... yellow fluorescent protein

LIST OF FIGURES

Figure 1.1: Modeling biological systems 2

Figure 2.1: Circuit diagram of the positive feedback network 14
Figure 2.2: GFP levels in the absence and presence of dox 15
Figure 2.3: Normalized fluorescence as a function of dox 16
Figure 2.4: Steady-state GFP expression levels versus dox 17
Figure 2.5: 50 hour equilibration period 20
Figure 2.6: Simulating the dynamic behavior of the network 22
Figure 2.7: Experimentally measured GFP expression levels 24
Figure 2.8: Percent activated cells over time 25
Figure 2.9: Temporal activation profile 28
Figure 2.10: Sensitivity of mean activation time 29
Figure 2.11: Sensitivity of variability in timing of activation 30
Figure 2.12: Steady-state dose response curves 35

Figure 3.1: Single negative feedback loop system 42
Figure 3.2: Pronounced oscillations in nuclear NF-κB levels for a system with a single IκBα-mediated negative feedback loop 43
Figure 3.3: Analysis of the characteristic period and the decay rate of oscillations produced by the IκBα-mediated negative feedback loop . 48
Figure 3.4: Time series of x for several values of τ_y and K 49
Figure 3.5: Dual negative feedback system 52
Figure 3.6: Damped oscillations with dual negative feedback 54
Figure 3.7: Representative experimental data for IκBα and IκBϵ synthesis delays and feedback strengths 56
Figure 3.8: Plot of R_m as a function of m 57
Figure 3.9: Response of the NF-κB signaling module to transient stimulation with magnitude $K = 2$ 59

Figure 3.10: Temporal dose response curves 60
Figure 3.11: Response of a no-feedback system with constitutive IκBα synthesis (a_y) increased from 0.00185 nM/min to 0.3 nM/min 61
Figure 3.12: Schematic of a phylogenetic tree showing organisms in which homologs for IκBα and IκBϵ were found using BLASTP 64
Figure 3.13: CV due to extrinsic variations in total NF-κB and due to extrinsic variations in IKK 66
Figure 3.14: CV for peak and late-phase nuclear NF-κB levels due to extrinsic and intrinsic fluctuations 68
Figure 3.15: Stochastic simulation results for the NF-κB network with 1000 total NF-κB molecules 70
Figure 3.16: Stochastic simulation results for the NF-κB network with 100,000 total NF-κB molecules 71
Figure 3.17: Comparison of stochastic and deterministic simulations 72
Figure 3.18: Alternative auto-repressive network 74

LIST OF TABLES

Table 2.1: Positive feedback circuit model variables 36
Table 2.2: Positive feedback circuit model reactions 36
Table 2.3: Positive feedback circuit model parameter values 37

Table 3.1: NF-κB model variables 85
Table 3.2: NF-κB model reactions 86
Table 3.3: NF-κB model parameter values 87
Table 3.4: Auto-repressor network reactions 88
Table 3.5: Auto-repressor network parameter values 88
Table 3.6: Organisms with homologs for IκBα 89
Table 3.7: Organisms with homologs for IκBϵ 91
Table 3.8: Genome status of organisms in Tables 3.6 and 3.7 93

ACKNOWLEDGEMENTS

I would like to acknowledge Dr. Jeff Hasty, Dr. Alex Hoffmann, and Dr. Lev Tsimring for their encouragement and enthusiasm. I would also like to thank my other committee members for their time and for the guidance they provided. I would like to acknowledge the members of the Systems Biodynamics Lab and the members of the Signaling Systems Lab for their support. Finally, I thank the National Science Foundation (NSF) for funding.

Chapter 1 contains material originally published as Longo D, Hasty J (2006) Dynamics of single-cell gene expression. *Mol Syst Biol* **2**: 64. The dissertation author was the primary investigator and author of this paper. Copyright permission to republish here was granted by Nature Publishing Group.

Chapter 2 contains material to be submitted as Longo D, Hoffmann A, Tsimring LS, Hasty J. Coherent activation of a synthetic mammalian gene network. *Syst Synth Biol.* The dissertation author was the primary investigator and author of this paper.

Chapter 3 contains material to be submitted as Longo D, Kearns JD, Hoffmann A, Hasty J, Tsimring LS. Dual delayed feedback provides sensitivity and robustness to the NF-κB signaling module. *Mol Syst Biol.* The dissertation author was the primary investigator and author of this paper.

VITA

2003 Bachelor of Science, University of Virginia

2005 Master of Science, University of California, San Diego

2009 Doctor of Philosophy, University of California, San Diego

PUBLICATIONS

Longo D, Kearns JD, Hoffmann A, Hasty J, Tsimring LS. Dual delayed feedback provides sensitivity and robustness to the NF-κB signaling module. *Mol Sys Biol* (to be submitted), 2009.

Longo D, Hoffmann A, Tsimring LS, Hasty J. Coherent activation of a synthetic mammalian gene network. *Sys Synth Biol* (to be submitted), 2009.

Longo D, Hasty J (2006) Dynamics of single-cell gene expression. *Mol Sys Biol* **2**: 64.

Longo D, Hasty J (2006) Imaging gene expression: tiny signals make a big noise. *Nat Chem Biol* **2**: 181-182.

Longo D, Peirce SM, Skalak TC, Davidson L, Marsden M, Dzamba B, DeSimone DW (2004) Multicellular computer simulation of morphogenesis: blastocoel roof thinning and matrix assembly in Xenopus laevis. *Dev Biol* **271**: 210-222.

Viola F, Longo D, Lawrence M, Walker W (2002) Analysis of clot formation with acoustic radiation force. *Proc SPIE* **4687**: 235-242.

FIELDS OF STUDY

Major Field: Bioengineering - Studies in Systems Biology

Professor Jeff Hasty, Dr. Lev S. Tsimring, and Professor Alex Hoffmann

ABSTRACT OF THE DISSERTATION

The Role of Feedback in Signaling Dynamics

by

Diane Marie Longo

Doctor of Philosophy in Bioengineering

University of California, San Diego, 2009

Jeff Hasty, Chair

This dissertation analyzes the dynamics of the individual components in two specific biological networks in order to understand how these components interact to produce observed cellular behavior.

First, we use an integrated experimental-computational approach to analyze the dynamical response of a synthetic positive feedback network in individual mammalian cells. Using flow cytometry, we observe a switch-like activation of the network with variable delay times in individual cells. In agreement with a stochastic model of the network, we find that increasing the strength of the positive feedback results in a decrease in the mean delay

time and a more coherent activation of individual cells. The results of this work are important for gaining insight into biological processes such as cell cycle regulation and apoptosis which rely on positive feedback to generate switch-like responses and may also facilitate the development of engineered mammalian control systems.

Second, we use computational modeling to study the dynamics of the NF-kappaB signaling pathway that governs mportant cellular processes such as inflammation and the immune response. Because the NF-kappaB pathway contains over 100 reactions, the complexity of this signaling network is enormous. Here, we utilize a modeling approach which replaces the complicated cascades of individual biochemical reactions by few compound but delayed reactions. We utilize both deterministic and stochastic formulations of our model to interrogate the negative feedback loops that regulate the dynamic activity of NF-kappaB. In agreement with our experiments, we find that the response of the dual-feedback circuit is tuned to minimize oscillations. Further, we reveal two important features of the dual-feedback-loop architecture that may explain its evolutionary advantage over no or single-feedback systems: first, it ensures a highly sensitive initial response while allowing for temporally graded outputs; and second, it minimizes stochastic fluctuations and leads to a robust response to incoming signals.

In conclusion, this dissertation investigates the behavior of both an artificial gene regulatory network and a naturally-occurring signaling network. This work involves the utilization of both computational and experimental techniques to gain insight into the dynamics of regulatory networks in mammalian systems.

Chapter 1

Introduction

1.1 Systems biology approach

Systems biology research focuses on examining the interactions between components in a biological system and understanding how these interactions give rise to the function and the dynamic behavior of that system (Kitano 2002). Following the maturation of high-throughput technologies that allow for large-scale analyses of DNA, RNA, and protein molecules (Duggan et al., 1999; Venter et al., 2001; Tannu and Hemby, 2006), systems-level approaches emerged to gain insight into the structure and function of complex biological networks. In the systems biology approach, both experimental and theoretical techniques are integrated to develop quantitative models of biological systems.

The first step in constructing a model of a biological system involves identifying the components in the biological system of interest (Figure 1.1A). In this stage, a "parts list" for the system is generated by identifying essential components such as proteins and gene regulatory elements that make up the system.

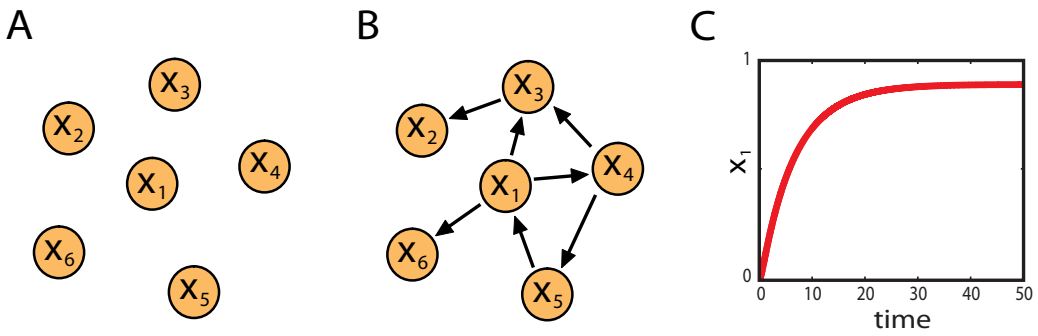

Figure 1.1: Modeling biological systems. (A) All of the components or nodes $(x_i, i = 1...n)$ in the biological network are identified. (B) Interactions between each of the components in the network are determined. (C) Mathematical model is used to simulate the temporal evolution of the network.

Next, all possible interactions between the components of the network must be identified (Figure 1.1B). Techniques such as yeast-two hybrid assays (Uetz 2002) and chromatin immunoprecipitation (Ren et al., 2000) can be used to discover protein-protein interactions and protein-DNA interactions respectively, and this interaction data can be used to predict the structure of gene regulatory networks and signaling pathways.

After both the components and the interactions between components in the biological system are identified, this information is used to develop a model that can predict the dynamic behavior of the network under various conditions or in response to perturbations (Figure 1.1C). Theoretical predictions must be tested experimentally, and experimental results can either validate the model prediction or discrepancies between model and experiment may indicate that further model refinement is necessary. This iterative process can generate novel insights into the structure-function relationships of biological networks.

In this work, we use the systems biology approach to interrogate the dynamic behavior of two specific biological networks: a synthetic mammalian positive feedback network and the NF-κB signaling module. We integrate experimental and computational methods to advance our understanding of how the components in these two networks interact to produce specific cellular behaviors.

1.2 Synthetic gene networks

The developing discipline of synthetic biology attempts to recreate in artificial systems the emergent properties found in natural biology (Hasty et al., 2002; Benner and Sismour 2005). Because the genetic circuits found in cells

are often highly integrated and quite complex, redesigning simpler synthetic systems for study is a valuable approach not only at the genome level but also at the gene network level. Recently, there has been significant activity directed towards designing synthetic gene networks that mimic the functionality of natural systems. In addition to being easier to construct, the reduced complexity and increased isolation of these networks makes them more amenable to both tractable experimentation and mathematical modeling (Sprinzak and Elowitz, 2005; Ferber 2004). The process of constructing and testing artificial systems resembling naturally occurring systems promises to advance our understanding of how biological systems function by providing information about cellular processes that cannot be obtained by studying intact native systems (Benner and Sismour, 2005; Ferber 2004; Endy 2005).

Simple gene modules, such as autoregulatory feedback loops (Becskei and Serrano, 2000; Becskei et al., 2001; Rosenfeld et al., 2002), toggle switches (Gardner et al., 2000; Atkinson et al., 2003), and oscillators (Elowitz and Leibler, 2000; Atkinson et al., 2003; Stricker et al., 2008), have been engineered in model microorganisms such as *E. coli* and *S. cerevisiae*. The behavior of these simple genetic circuits has been observed in vivo by using flow cytometry or fluorescence microscopy to measure reporter protein levels in individual live cells.

Synthetic gene networks have been constructed to demonstrate the ability of negative feedback to reduce cell-to-cell fluctuations in protein concentrations, thus increasing the stability of the network (Becskei and Serrano, 2000). Positive feedback loops amplify cellular fluctuations and allow for the generation of bistability (Savageau, 1974). Bistability, or the existence of two stable

states, has been observed in a synthetic positive feedback system (Becskei et al., 2001). Two distinct populations of cells were observed by fluorescence microscopy: cells that expressed low levels of GFP and cells that expressed high levels of GFP. Stochastic fluctuations in the network enabled spontaneous transitions from one expression state to the other.

Simple, well-characterized gene modules can be linked to form more complex networks. A recent study designed and constructed a repressor-only system, an activator-only system, and a system that combines the activator and repressor modules (Guido et al., 2006). A stochastic model accurately predicted the behavior of the modular system. The study demonstrated that the properties of individual regulatory modules can be used to predict the behavior of more complex gene regulatory networks, setting the stage for the systematic construction of synthetic gene networks of increasing complexity, which mimic the behavior of naturally occurring systems.

The behavior of synthetic gene networks can often be characterized by obtaining distributions of cellular reporter protein levels at various time points. For instance, Gardner et al. (2000) used this approach to analyze a synthetic genetic toggle switch. The bistability of the synthetic network was demonstrated by showing that transient chemical or thermal induction could switch *E. coli* cells from one stable state corresponding to high expression of a GFP reporter to a second stable state corresponding to low GFP expression levels. Flow cytometry was used to measure GFP expression levels from individual cells and GFP distributions were obtained to show the existence of a stable low GFP expressing state and a stable high GFP expressing state. A bimodal distribution appears as switching begins, and the return to a unimodal

distribution occurs when switching is complete.

The development of inducible mammalian transgene control systems has enabled the construction of synthetic gene circuits in mammalian systems (Greber and Fussenegger, 2007). Recently, mammalian transgene control elements have been utilized to engineer synthetic mammalian networks such as toggle switches (Kramer et al., 2004), hysteretic switches (Kramer and Fussenegger, 2005), and time-delay circuits (Weber et al., 2007).

In Chapter 2, we use synthetic biology techniques to construct a simple mammalian autoregulatory network. We use an integrated experimental-computational approach to analyze the dynamic response of the synthetic network in individual cells.

1.3 Stochastic gene expression

Cellular heterogeneity has been observed in a wide variety of cell types ranging from simple bacterial cells (Ozbudak et al., 2002; Swain et al., 2002) to more complex mammalian cells (Ramsey et al., 2006). Any population of cells will exhibit some degree of variability, and genetic differences are one of the main factors responsible for cellular heterogeneity. However, variation is also present in genetically identical cell populations, even when the cells have been exposed to the same environment and have the same history (Elowitz et al., 2002; Rao et al., 2002; Blake et al., 2003; Raser and O'Shea, 2005). Noise, or random fluctuations, in the process of gene expression is thought to contribute to this phenotypic variation.

Single-cell measurements are necessary for investigating the stochastic nature of gene expression because cell-to-cell variation can not be quantified

using population level measurements. Noise in gene expression arises from not only the inherent randomness of biochemical processes such as transcription and translation, but also from the fluctuations in cellular components that lead indirectly to variation in the expression of a particular gene (Swain et al., 2002). The total noise in the level of expression of a given gene can be divided into intrinsic and extrinsic components. Extrinsic noise arises from fluctuations in cellular components such as regulatory proteins and polymerases and has a global effect (Elowitz et al., 2002). Intrinsic noise arises from the stochastic nature of the biochemical process of gene expression and causes identical copies of a gene to express at different levels (Elowitz et al., 2002).

Single-cell studies have been key in gaining insight into the stochastic nature of gene expression. Such studies often involve monitoring the level of a protein expressed from an engineered gene circuit in individual live prokaryotic or simple eukaryotic cells. For example, Ozbudak et al. used point mutations to independently vary the transcriptional and translational rates of a single-gene network in *B. subtilis* and found that fluctuations in the level of a fluorescent reporter gene increased linearly with translational efficiency (Ozbudak et al., 2002). The results were consistent with a stochastic model that predicted that noise for a single gene is determined at the translational level (Thattai and van Oudenaarden, 2001). Elowitz et al. developed a method utilizing two different fluorescent proteins expressed from identical promoters to study noise in gene expression in *E. coli* (Elowitz et al., 2002). This study demonstrated that noise in gene expression results in fluctuations in protein levels in a clonal population and both intrinsic and extrinsic noise contribute to total noise in gene expression. Raser and O'Shea modified the dual-reporter

method to measure gene expression in the yeast *S. cerevisiae* and found that gene expression variability is dominated by extrinsic noise (Raser and O'Shea, 2004). More recently, Bar-Even et al. utilized 43 strains from the yeast GFP clone collection to analyze cell-to-cell variation in gene expression in *S. cerevisiae* (Bar-Even et al., 2006). The study measured protein noise and mean protein abundance for each of the fusion proteins subjected to 11 different environmental conditions and discovered a strong correlation between cell-to-cell variability and mean expression level. Theoretical analysis of these results suggests that sources intrinsic to the biochemical process of gene expression make a substantial contribution to gene expression noise (Bar-Even et al., 2006). Another large-scale study of gene expression noise was recently performed by utilizing high-throughput flow cytometry to measure protein abundances in a collection of GFP-tagged yeast strains (Newman et al., 2006). This study also observed a global relationship between noise and protein abundance suggesting that intrinsic noise dominates gene expression noise (Newman et al., 2006). The global trend observed between protein noise and mean abundance does not extend to regions of high protein abundance (Bar-Even et al., 2006; Newman et al., 2006) thus explaining the apparent discrepancy between the recent large-scale results (Bar-Even et al., 2006; Newman et al., 2006) and the results of Raser and O'Shea which utilizes a highly abundant reporter gene.

Recent single-cell experiments have provided further insight into cell-to-cell variability by examining how noise in gene expression propagates from one gene to the next (Pedraza and van Oudenaarden, 2005), measuring the relative amplitude and time scales of intrinsic and extrinsic noise (Rosenfeld et al., 2005), analyzing the relative contribution of global noise and pathway-

specific noise to variation in a cell-fate decision (Colman-Lerner et al., 2005), investigating the relationship between gene circuit structure and noise frequency range (Austin et al., 2006), examining the effects of cell-cycle position on cell-to-cell variation (Colman-Lerner et al., 2005) and on nuclear protein levels and localization (Sigal et al., 2006), and investigating the source of extrinsic noise in eukaryotic gene expression (Volfson et al., 2005). (For a review of the origins and consequences of noise in gene expression see McAdams and Arkin, 1999; Kaern et al., 2005; Raser and O'Shea, 2005).

In Chapter 2, we examine cell-to-cell variability in the timing of activation of a synthetic mammalian positive feedback network. In agreement with a stochastic model of the network, we find that a more coherent activation of individual cells is achieved with strong positive feedback.

In Chapter 3, we examine variability in the response of the NF-κB signaling module. We demonstrate that dual feedback loops allow for a more robust response than a single feedback loop system. In addition, we reveal that variability in the NF-κB response is dominated by extrinsic noise for large systems ($>$ 10,000 NF-κB molecules), while intrinsic noise becomes more significant for much smaller systems ($<$ 1,000 NF-κB molecules).

1.4 Acknowledgements

Chapter 1 contains material originally published as Longo D, Hasty J (2006) Dynamics of single-cell gene expression. *Mol Syst Biol* **2**: 64. The dissertation author was the primary investigator and author of this paper. Copyright permission to republish here was granted by Nature Publishing Group.

Chapter 2

Coherent activation of a synthetic mammalian gene network

2.1 Introduction

Positive feedback regulation plays an important role in many cellular signaling systems. Biological processes such as cell cycle regulation (Yao et al., 2008; Skotheim et al., 2008), apoptosis (Legewie et al., 2006), and vertebrate oocyte maturation (Ferrell and Machleder, 1998) rely on positive feedback to generate a bistable switch in which cells transition from one distinct phenotype to another while residing in intermediate states only transiently. In these systems, cell-to-cell variability within a population of cells can result in a non-uniform response with individual cells switching between states at different times following induction (Rehm et al., 2002; Lai et al., 2004). A quantitative analysis of the dynamic behavior of positive feedback modules at the single-cell level may provide insight into how information flows through such motifs and can lead to a greater understanding of the switch-like responses that occur in

many regulatory systems.

Characterizing the behavior of individual positive feedback modules in naturally occurring signaling pathways is difficult because these positive feedback loops are often embedded in extremely complicated networks. In contrast, simple engineered gene networks consisting of a single positive feedback loop can be analyzed as isolated regulatory modules. Several simple synthetic gene networks have been engineered and analyzed in model organisms such as *E. coli* and *S. cerevisiae* (Elowitz et al., 2002; Raser and O'Shea, 2004; Volfson et al., 2005). The recent development of inducible mammalian transgene control systems has allowed for the construction of synthetic gene circuits in mammalian cells and organisms (Greber and Fussenegger, 2007). Mammalian transgene control elements have been used to build synthetic mammalian networks such as toggle switches (Kramer et al., 2004), hysteretic switches (Kramer and Fussenegger, 2005), and time-delay circuits (Weber et al., 2007). Most of these engineered mammalian networks have been characterized using steady-state population level measurements hindering an examination of the dynamic network behavior in individual cells (Longo and Hasty, 2006). Obtaining quantitative single-cell measurements using fluorescence-activated cell sorting (FACS) is a valuable approach for analyzing gene expression levels in individual cells. In a recent study, the hysteretic response of a synthetic mammalian positive feedback network was monitored with single-cell FACS measurements allowing a bimodal response profile to be observed (May et al., 2008).

Some of the most widely used mammalian gene control systems are those which are regulated with tetracycline or the tetracycline analogue doxy-

cycline (Gossen and Bujard, 1992; Gossen et al., 1995; Rennel and Gerwins, 2002). Here, we construct a synthetic mammalian positive feedback gene regulatory network using tetracycline-responsive control elements, and we utilize an integrated experimental-computational approach to analyze the dynamic response of the network at the single-cell level. Using a stochastic model of the network, we demonstrate that increasing the strength of the positive feedback results in a shorter mean delay time prior to activation and less variability in the activation time in individual cells. We confirm our theoretical predictions with quantitative single-cell measurements from a clonal population of mammalian cells harboring the synthetic circuit. Our findings may help us to predict the dynamic behavior of more complex cellular networks and may improve our ability to construct artificial gene networks that could be useful for gene therapy.

2.2 Design and construction of a synthetic mammalian positive feedback network

We have constructed a mammalian synthetic gene network that utilizes tetracycline (tet) responsive control elements. The synthetic network (Figure 2.1) consists of two vectors: (i) an autoregulatory vector which contains the coding sequence for a tet-responsive transactivator (rtTA) downstream of an O7-CMVm tet-regulatable promoter and (ii) a reporter vector which contains the *gfp* gene downstream of the O7-CMVm promoter. In the presence of doxycycline (dox), rtTA binds to tet operator sites on each O7-CMVm promoter thereby inducing its own expression and expression of the GFP (green fluorescent protein) reporter. The binding affinity of rtTA to the tet operator

sites is determined by the concentration of dox. Thus, the strength of the positive feedback can be tuned by altering the concentration of dox. Stable mammalian cells harboring the synthetic circuit were generated by transducing mouse embryonic fibroblasts (NIH 3T3 cells) with the two vectors. Clonal populations were produced by single-cell sorting the transduced cells and expanding individual cells into stable clonal cell lines. Cell lines were screened for inducibility by using flow cytometry to measure GFP expression levels from each clone after being cultivated in the absence and presence of dox (1 μg/ml for 24 hours). GFP expression levels from a representative clone are shown in Figure 2.2.

In all of the clones assayed, mean GFP expression increased with the addition of dox. We selected one clone for further quantitative analysis. The response of the clone to several dox concentrations was examined by culturing cells in dox concentrations ranging from 0 to 1 μg/ml for 3 days and measuring fluorescence levels using flow cytometry (Figure 2.3). Because mean fluorescence levels do not reach steady state values within 3 days of induction, the dose-response curve in Figure 2.3 represents a transient response of the system. Simulated steady-state GFP expression levels as a function of dox (Figure 2.4) reveal that the system is bistable for a small range of dox concentrations.

2.3 Stochastic modeling of the mammalian synthetic network

Cell-to-cell variability is present in any population of cells including genetically identical cell populations that have been exposed to the same environment (Elowitz et al., 2002; Raser and O'Shea, 2005). Gene expression

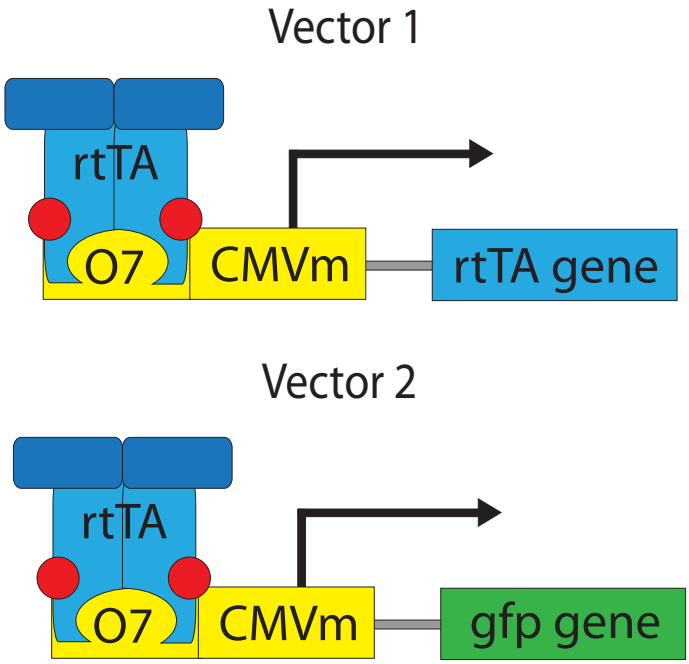

Figure 2.1: Circuit diagram of the positive feedback network. The O7-CMVm inducible promoter consists of seven operator sites (O7) fused to a minimal CMV promoter (CMVm). Vector 1 contains the *rtTA* gene downstream of the inducible promoter. Vector 2 contains the *gfp* gene downstream of the inducible promoter. In the presence of tetracycline, the rtTA dimers bind to the tet operator sites on the regulatable promoters and induce expression of rtTA and GFP.

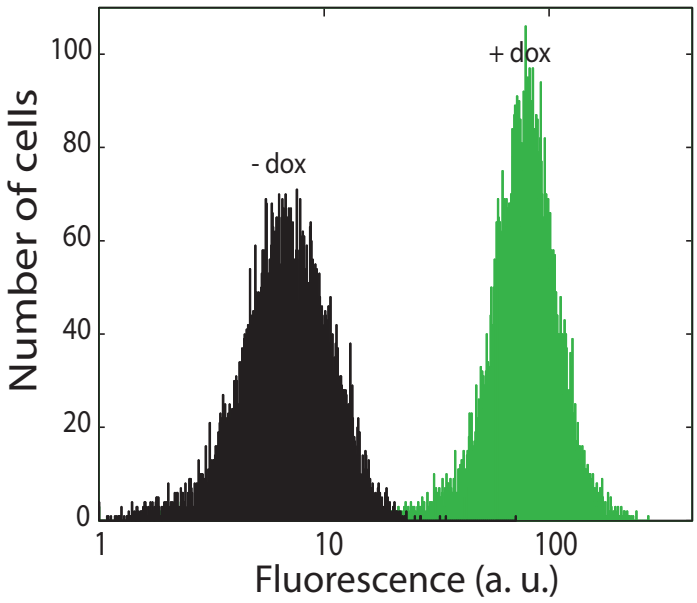

Figure 2.2: GFP levels in the absence and presence of dox. GFP expression levels were measured for a mammalian cell line harboring the synthetic network in the absence of dox (black) and in the presence of 1 μg/ml dox (green) for 24 hours.

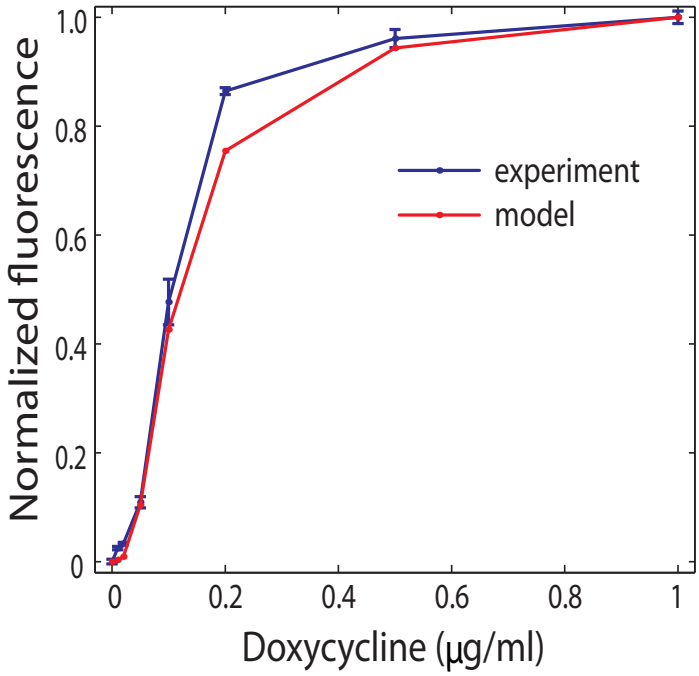

Figure 2.3: Normalized fluorescence as a function of dox. Experimental GFP expression levels were determined by FACS after cells from a clonal population were cultured in each dox concentration for 3 days. Error bars represent standard deviation of triplicate samples. Theoretical mean expression levels were determined from 20 runs of the simulation following induction at each dox concentration for 3 days. Experimental and theoretical data were individually normalized to conditions of no induction (0 μg/ml dox) and full induction (1 μg/ml dox).

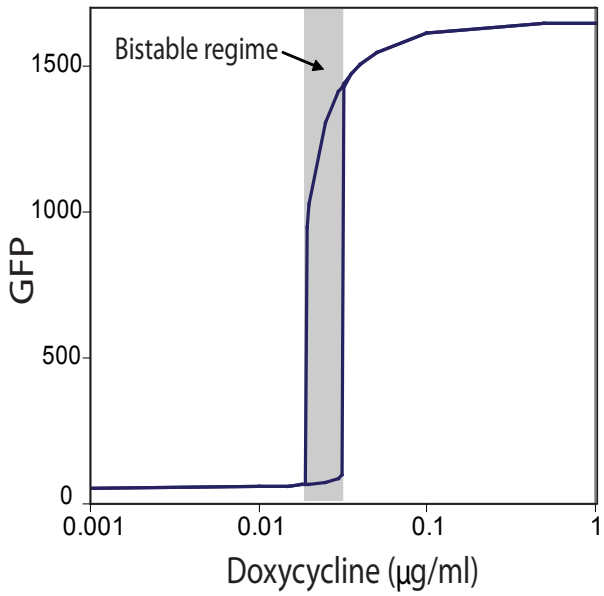

Figure 2.4: Steady-state GFP expression levels versus dox. A deterministic model (described in Materials and Methods) derived from the network reactions listed in Table 2.2 was used to determine stable steady-state GFP levels.

noise arising from the inherent randomness of biochemical processes such as transcription and translation can lead to cell-to-cell variation in the expression of a gene (Raj and van Oudenaarden, 2008). To facilitate our exploration of the synthetic networks dynamic behavior at the single-cell level, we used the Gillespie algorithm (Gillespie, 1977) to perform stochastic simulations of the biochemical reactions involved in the positive feedback network. The model reactions include transcription, translation, mRNA degradation, and protein degradation of both the activator (rtTA) and the GFP reporter (Table 2.2). rtTA dimerization and operator binding are reflected in the transcriptional rates which are described by Hill-type functions. The association constant of the activator, K_a, is determined by $K_a = S/(K_s + S)$ where S is the dox concentration and K_s is the dox concentration that results in half-maximal K_a. The binding affinity of rtTA to the tet operator sites, and thus the strength of the positive feedback, is highest at high dox concentrations. Model parameter values were estimated using values in the literature where available, and remaining parameter values were chosen such that the model generates a dose-response curve that is in good agreement with experimentally observed dose-response behavior (Figure 2.3, Table 2.3). All stochastic simulations were equilibrated for a period of 50 hours to allow variability in expression levels to stabilize prior to induction with dox. We used the coefficient of variation (CV, standard deviation divided by the mean) to quantify variability in GFP levels and found that the CV plateaus at approximately .35 (Figure 2.5). We verified that the experimental level of cell-to-cell variability in the uninduced state is similar to that seen in our model by analyzing GFP expression levels determined by flow cytometry for cells cultured in the absence of dox. We found

that the experimentally determined CV has a value of .43 and thus agrees well with the CV for the simulations. This level of cell-to-cell variability falls within the range in CV (.1 to .6) that was recently reported for nearly 1000 protein levels in human cells (Cohen et al., 2008).

2.4 Coherent activation with strong positive feedback

Using our stochastic model, we examined how the strength of the positive feedback affects the response of the network in individual cells with variable expression levels. Stochastic simulations were run to observe the dynamic behavior of the network following induction with .05, .1, and 1 μg/ml dox. Because these dox concentrations are all above the bistable regime (Figure 2.4), all trajectories will eventually reach a steady state with high GFP expression levels. At the lowest dox concentration, .05 μg/ml, the association constant K_a is below half-maximal ($K_a = .38$) resulting in weak positive feedback. At .1 μg/ml dox, K_a is near half-maximal ($K_a = .56$) resulting in intermediate strength positive feedback, and at 1 μg/ml dox, the strength of the positive feedback is near maximal with $K_a = .93$. Our simulated results reveal that, at each of the three concentrations, there is a switch-like activation of the network with individual trajectories flipping to the high GFP steady state at different times following induction with dox (Figure 2.6). At the lowest dox concentration (.05 μg/ml), there is a mean delay of approximately 50 hours before switching occurs (Figure 2.6A). This mean delay time decreases as the positive feedback strength increases, with cells beginning to flip to the high expressing state within 10 hours following induction at the highest dox

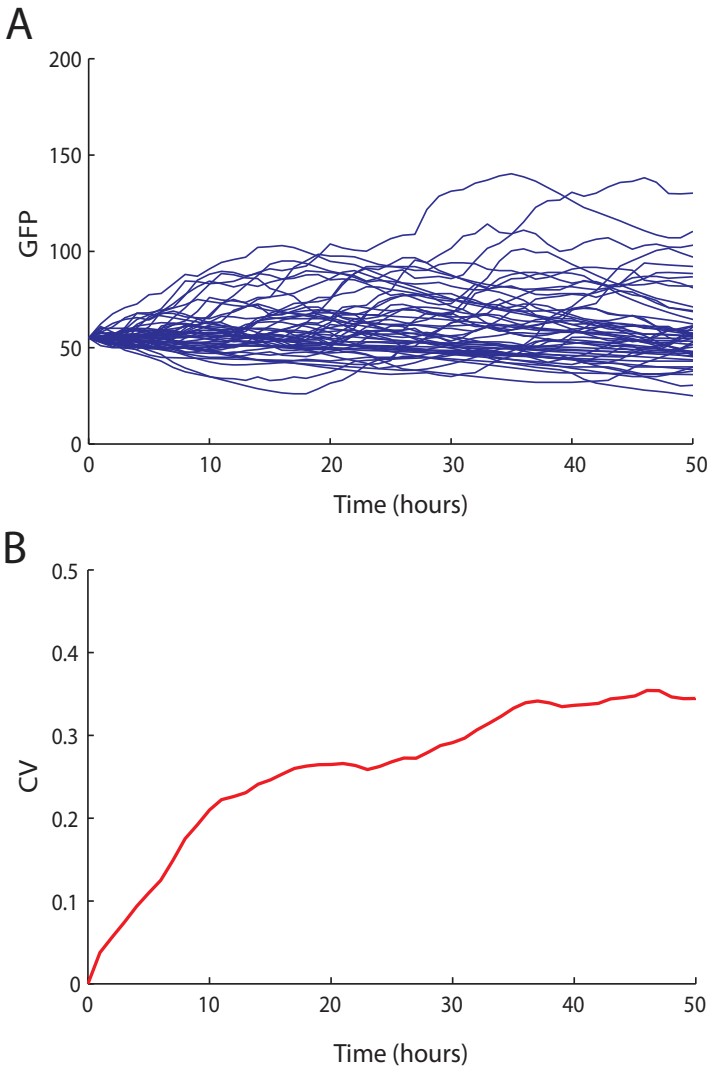

Figure 2.5: 50 hour equilibration period. mRNA and protein levels were initialized to their basal steady state values at $t = 0$ and the stochastic simulations were run for 50 hours with no dox ($S = 0$). (A) GFP levels for 50 individual runs of the stochastic simulation during the model equilibration period. (B) The coefficient of variation (CV) for 50 simulations.

concentration (Figure 2.6C). The simulations also reveal that the timing of activation is extremely variable with low feedback strengths. In response to induction with .05 μg/ml dox, some trajectories start to switch to the high expression state as early as 50 hours following induction while a significant fraction of the population is still expressing GFP at low basal levels at 200 hours following induction (Figure 2.6A). At .1 μg/ml, there is a smaller time window during which activation occurs ranging from approximately 20 hours to 100 hours following induction (Figure 2.6B). With strong positive feedback (1 μg/ml dox), there is a more coherent activation, with all trajectories beginning to switch to the high state within approximately 40 hours (Figure 2.6C).

To test our theoretical predictions, we employed flow cytometry to examine the temporal response of the network following induction with .05, .1, and 1 μg/ml dox. We measured the GFP expression levels of cells that were cultured in each dox concentration for 0, 10, 20, 30, 40, and 50 hours. Following induction, fluorescence histograms show bimodality (Figure 2.7) thus confirming that there is a switch-like activation of the network. At each dox concentration, the percentage of cells with high expression levels increased over time. However, in agreement with our theoretical results, the dynamics of activation differed significantly for the three dox concentrations. Our measurements confirm our theoretical prediction that low feedback strengths result in a longer mean delay time prior to activation. The fluorescence distribution does not start to appear bimodal until 40 hours following induction at the lowest feedback strength (.05 μg/ml dox). In contrast, at 1 μg/ml dox, activation is much more rapid with a bimodal distribution appearing within 10

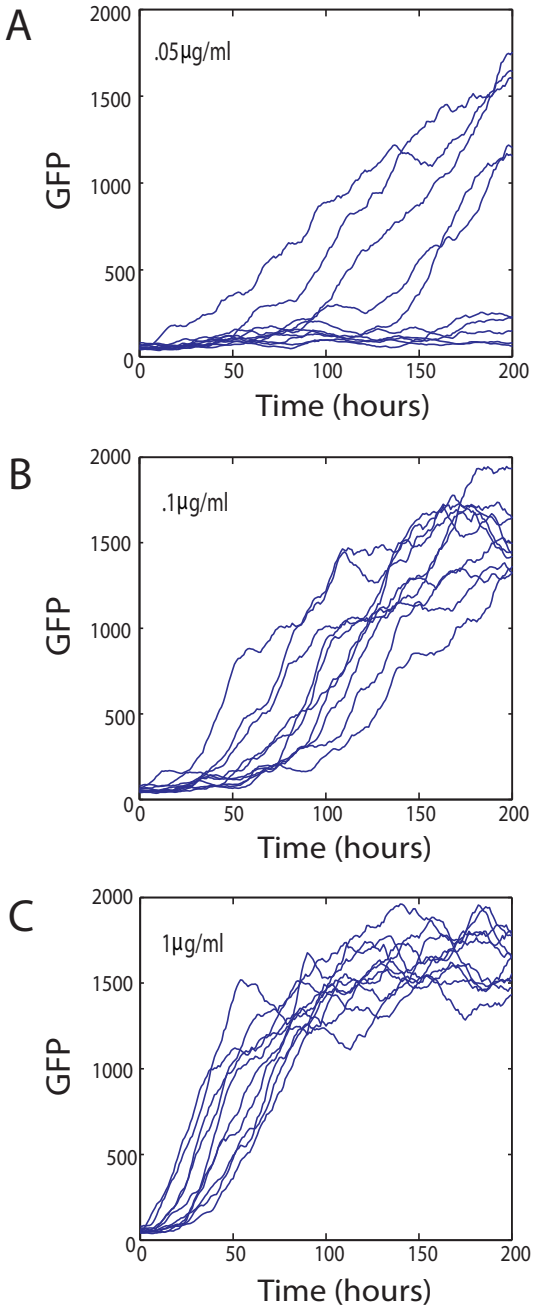

Figure 2.6: Simulating the dynamic behavior of the network. The plots show ten typical runs of stochastic simulations in response to .05 μg/ml dox (A), .1 μg/ml dox (B), and 1 μg/ml dox (C).

hours following induction. Our experimental results also confirm that there is indeed less variability in the timing of activation in individual cells with strong positive feedback. This can be seen more clearly by examining the percentage of activated cells at each time point (Figure 2.8). At 1 μg/ml dox, about 90 percent of the cells are activated within 30 hours. In contrast, at .05 and .1 μg/ml dox, there is a more gradual increase in the percentage of activated cells at each time point. The percentage of high expressing cells over time as determined by the model is also shown in Figure 2.8. We find that there is a good agreement between our simulations and our experimental data.

2.5 Naturally-occurring regulatory networks with positive feedback

Our theoretical and experimental analysis of a simple mammalian positive feedback module has revealed that there is a variable delay time prior to the switch-like activation of the network, with the longest delay times and the least coherent activation occurring when the positive feedback strength is low. Similar signaling response characteristics have been observed in several naturally-occurring regulatory networks that contain positive feedback regulation. In *S. cerevisiae*, positive feedback in the G1/S regulatory network allows for a switch-like activation into cell cycle entry with a coordinated activation of individual cells, while a more discordant response is observed when positive feedback is completely removed from the network (Skotheim et al., 2008). Single-cell studies have shown that cell cycle entry in mammalian cells is also governed by a network which generates an all-or-none response via positive feedback regulation (Yao et al., 2008). However, quantifying the timing of

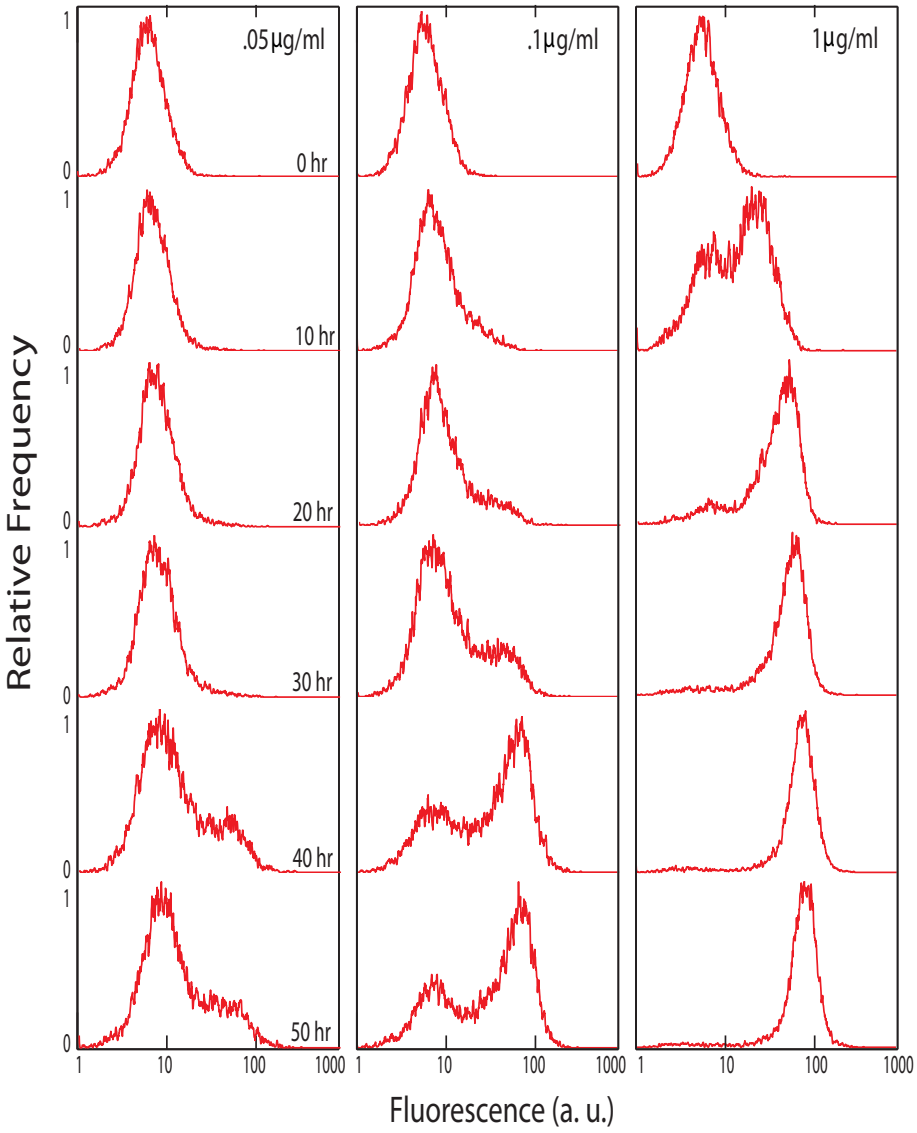

Figure 2.7: Experimentally measured GFP expression levels. Fluorescence distributions from cells induced with .05, .1, or 1 μg/ml dox for 0, 10, 20, 30, 40, and 50 hrs. The relative frequency was obtained by normalizing the actual frequency by the frequency at the mode.

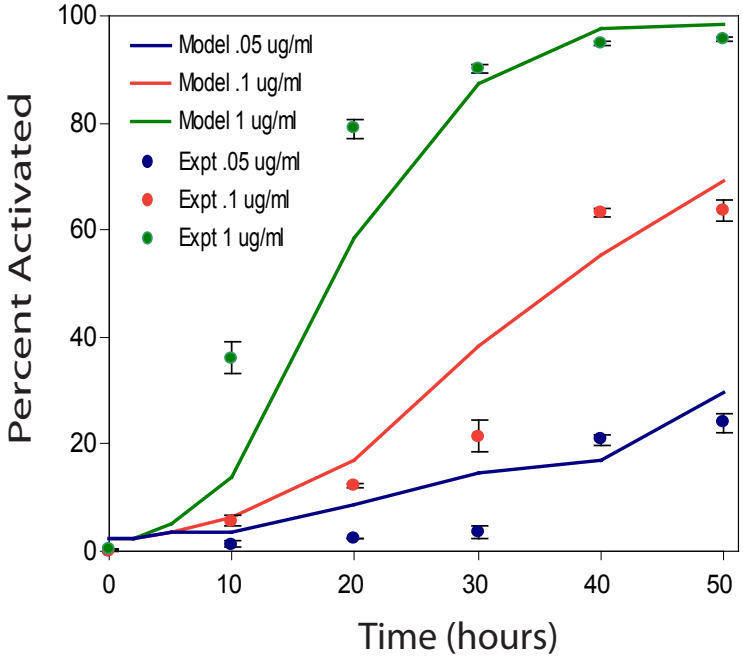

Figure 2.8: Percent activated cells over time. The percentage of cells in the activated state was determined from flow cytometry measurements. Error bars represent standard deviation of triplicate samples. Theoretical values were determined from 200 runs of the simulation at each concentration.

cell cycle entry in single cells will be necessary to determine if there is also a coherent activation into cell cycle entry in mammalian cells.

In the signaling pathway that governs apoptosis, positive feedback is utilized to generate an all-or-none activation of the effector caspases which provoke cell death (Legewie et al., 2006), and the timing of effector caspase activation has been shown to vary considerably in individual mammalian cells (Rehm et al., 2002; Albeck et al., 2008). Although the delay time is variable and relatively long (several hours), once activated, effector caspases cleave their substrates and provoke cell death within minutes (Goldstein et al., 2000; Rehm et al., 2002). Thus, the response of effector caspases can be divided into two temporal components: a long and variable delay followed by a short and relatively robust period of activity. We next asked whether a complex regulatory architecture was necessary for producing this type of response, or if a simple positive feedback module could generate a similar response profile.

To address this question, we utilized our experimentally-validated stochastic model to examine the mean and standard deviation in the first and second portion of the response of our synthetic autoregulatory network. We define the first portion of the response (τ_1) as the time period required for GFP expression levels to surpass basal expression levels (and thus exceed a lower threshold value), and we define the second portion of the response (τ_2) as the time period required for GFP levels to increase from the lower threshold value to the maximum expression level (and thus exceed an upper threshold value) (Figure 2.9A). The mean and standard deviation for τ_1 and τ_2 were determined from 50 simulations at several dox concentrations (Figure 2.9B). We find that τ_1 is highly dependent on the dox concentration (τ_1 approaches infinity as the

dox concentration approaches the bistable regime where some trajectories can remain in the low state indefinitely (Figure 2.4)). In contrast, (τ_2) is rather insensitive to changes in dox. At dox concentrations below .1 μg/ml, τ_1 has a higher mean and standard deviation than τ_2. Thus, in this regime, there is a relatively long and variable delay period followed by a shorter, less variable period of activation. Therefore, the simple synthetic positive feedback network is in fact capable of generating a response profile that is similar to the apoptotic response.

We next investigated how the timing of activation (τ_1) is affected by changes in the parameter values which determine the levels of the transactivator by performing a parameter sensitivity analysis. In our model, each of the parameter values involved in rtTA synthesis and degradation were increased and decreased by 5% (with a dox concentration of 1 μg/ml) and the change in the mean value of τ_1 was determined (Figure 2.10). We find that the timing of activation is most sensitive to changes in the basal transcription rate of rtTA (α_A) and the fold-induction of transcription (f). With a 5% decrease in α_A, the mean time of activation is increased by over 12 hours (an increase of over 16%). Variability in the timing of activation (determined by the standard deviation in τ_1) also depends strongly on the values of the transcriptional parameters α_A and f (Figure 2.11). These results demonstrate that the timing of activation depends not only on the strength of the feedback but also depends strongly on the basal and induced transcription rates. In naturally-occurring regulatory networks such as the network governing apoptosis, precise regulation of these transcriptional rates may provide a mechanism for tuning the timing of activation.

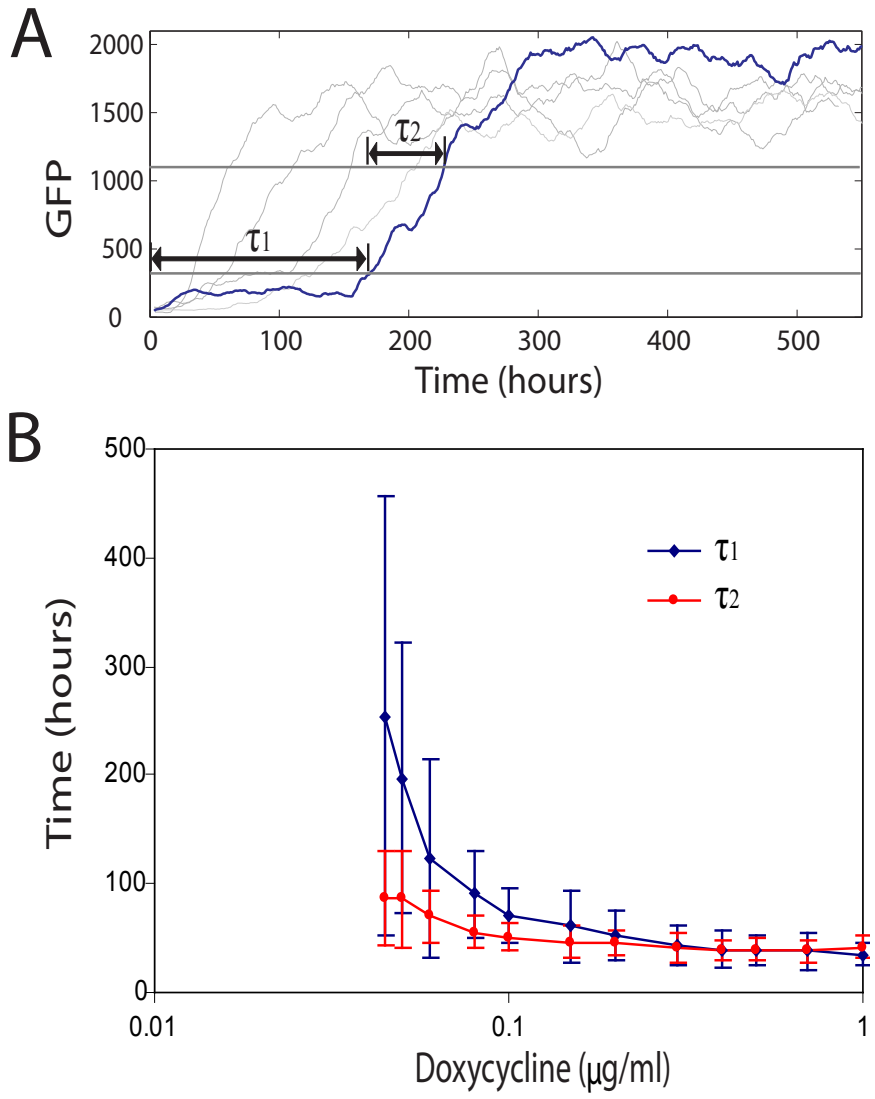

Figure 2.9: Temporal activation profile. (A) Five simulated trajectories are shown to demonstrate the lower and upper thresholds used for calculating τ_1 and τ_2. The length of τ_1 and τ_2 are shown for the blue trajectory (B) Mean and standard deviation for τ_1 and τ_2 versus dox for 50 simulations.

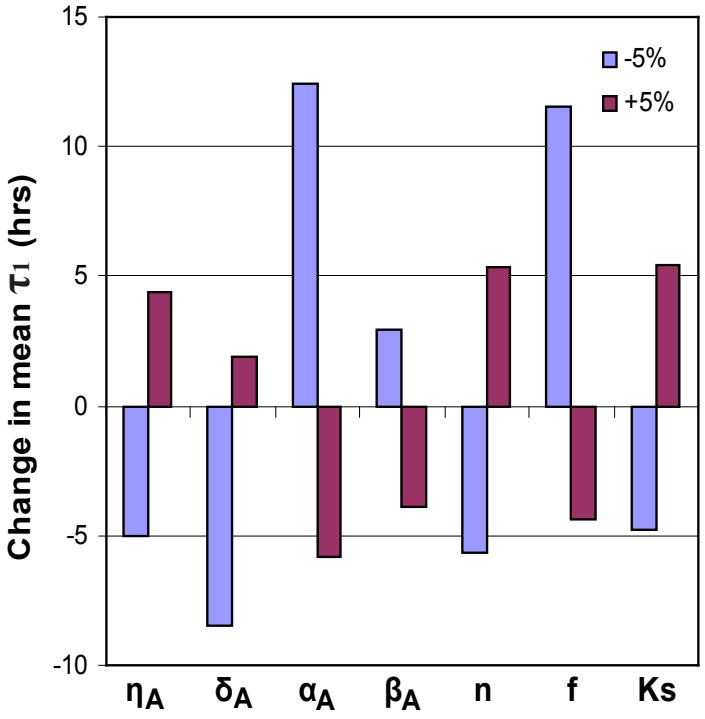

Figure 2.10: Sensitivity of mean activation time. In the parameter sensitivity analysis, each of the parameters involved in the production and degradation of rtTA mRNA and protein levels were increased and decreased by 5% (with $S = 1$ μg/ml). The corresponding change in the mean time of activation (τ_1) for 50 individual runs of the stochastic simulation is plotted.

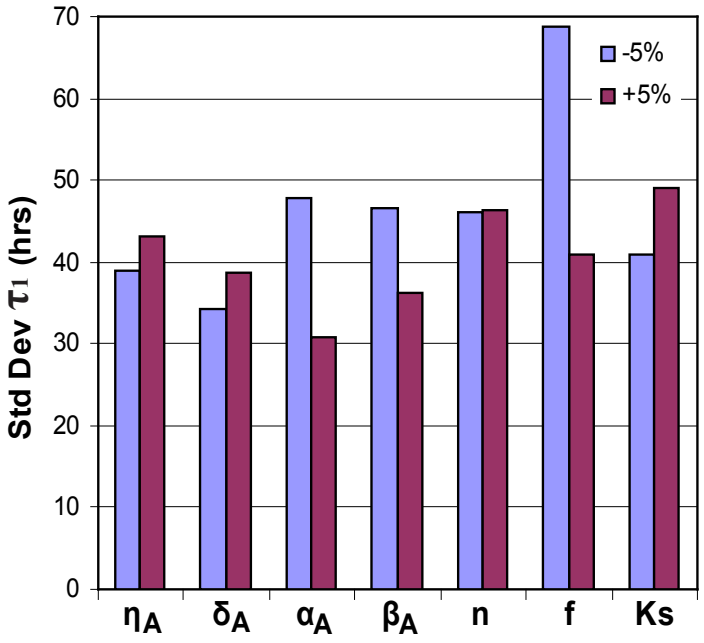

Figure 2.11: Sensitivity of variability in timing of activation. In the parameter sensitivity analysis, each of the parameters involved in the production and degradation of rtTA mRNA and protein levels were increased and decreased by 5% (with $S = 1$ μg/ml). The standard deviation in the time of activation (τ_1) for 50 individual runs of the stochastic simulation is plotted.

2.6 Discussion

In this work we have utilized an integrated computational-experimental approach to analyze the dynamic response of a synthetic mammalian positive feedback network at the single-cell level. We have demonstrated that the switching-time characteristics of the synthetic network are highly dependent on the strength of the feedback with the shortest mean delay time and the most coherent response being produced by strong positive feedback.

The signaling properties of the simple synthetic positive feedback network are similar to signaling response characteristics that have been observed in several naturally-occurring, complex regulatory networks that contain positive feedback regulation. Using our experimentally-validated stochastic model we investigated whether or not our simple circuit could recapitulate the two temporal phases involved in caspase activation, and we found that the simple positive feedback module could in fact produce a similar temporal response profile. Using a parameter sensitivity analysis, we found that the timing of activation is highly sensitive to changes in the transcriptional rates of the transactivator. In naturally-occurring regulatory networks, this dependence on transcriptional levels may allow for precise regulation of the timing of activation.

The approach used here to characterize the dynamic response of a simple engineered mammalian regulatory network can be utilized to provide greater insight into the signaling properties of the more complicated regulatory networks found in living cells and may also facilitate the development of engineered mammalian control systems.

2.7 Materials and Methods

2.7.1 Network construction

The GFP reporter vector, Hermes-HRSpuro-gfp (Rossi et al., 1998), was a gift from Helen Blau, Blau Laboratory, Stanford University, Stanford, CA. The autoregulatory vector was constructed from Hermes-HRSpuro-gfp by replacing the coding sequence for GFP with the coding sequence for the tet-responsive transactivator (rtTA). Oligonucleotide primers were used to PCR amplify the *rtTA* gene from the RTAb(+) vector (Rossi et al., 1998) (a gift from Helen Blau, Blau Laboratory, Stanford University, Stanford, CA) and restriction endonucleases and T4 DNA ligase was used to insert the *rtTA* gene downstream of the O7-CMVm promoter. Plasmids were propagated in *E. coli* cells grown in LB and the antibiotic ampicillin. Cloning was confirmed by restriction digests visualized by gel electrophoresis, and the constructed vector was verified by utilizing the sequencing service provided by Eton Bioscience, Inc. The autoregulatory vector and the reporter vector were purified using Qiagens Plasmid Midi Kits.

2.7.2 Cell culture

NIH 3T3 cells were maintained in DMEM supplemented with 10% bovine calf serum, penicillin (100 units/ml), streptomycin (100 μg/ml), and L-glutamine (1%). Cells were grown in a 5% CO_2, 37°C incubator.

2.7.3 Retroviral transductions

Retroviral constructs were cotransfected with pCL.Eco into 293T cells, and 42 hr posttransfection filtered supernatant was used to infect NIH 3T3

cells. Low efficiency infections (infection rates less than 2%) were used to ensure single copy integration per cell. To generate cells harboring both vectors, cells were first infected with the autoregulatory vector and selected with puromycin hydrochloride (Sigma). Selected cells were subsequently superinfected with the reporter vector and GFP-positive cells were sorted by FACS.

2.7.4 Flow cytometry

Cells were washed in phosphate-buffered saline (PBS) and resuspended in PBS. Cells were sorted using a Becton-Dickinson FACSVantage SE flow cytometry system. Cells were analyzed with a Becton-Dickinson FACSCalibur flow cytometer with a 488-nm argon excitation laser and a 515-545-nm emission filter (FL1) at a high flow rate. Forward scatter values and fluorescence values were collected for at least 10,000 cells per sample. Data analysis was performed using MATLAB (the MathWorks, Inc.). A forward-scatter and side-scatter gate was used to minimize fluorescence variation due to cell size.

2.7.5 Modeling the synthetic network

Stochastic simulations of the reactions in Table 2.2 were performed by implementing the Gillespie algorithm (Gillespie, 1977) in C++.

The deterministic model of the synthetic positive feedback network was implemented in MATLAB (the MathWorks, Inc.). The deterministic model consists of the following four ordinary differential equations describing the levels of rtTA mRNA (m_A), rtTA protein (A), GFP mRNA (m_G), and GFP protein (G):

$$\dot{m}_A = \frac{\alpha_A(1 + f(AK_a)^n)}{1 + (AK_a)^n} - \eta_A m_A \tag{2.1}$$

$$\dot{A} = \beta_A m_A - \delta_A A \tag{2.2}$$

$$\dot{m}_G = \frac{\alpha_G(1 + f(AK_a)^n)}{1 + (AK_a)^n} - \eta_G m_G \tag{2.3}$$

$$\dot{G} = \beta_G m_G - \delta_G G \tag{2.4}$$

where α_A and α_G represents the basal synthesis rates of A and G respectively, β_A and β_G represent the protein production rates of A and G respectively, f represents the fold-difference between basal and fully activated synthesis, n represents the Hill coefficient for activator dimers binding to tet operator sites, η_A and η_G represent the mRNA degradation rates of A and G respectively, δ_A and δ_G represent the protein degradation rates of A and G respectively, and K_a represents the association constant of the activator which is determined by the doxycycline concentration (S) via $K_a = S/(K_s + S)$. Note that the region of bistability determined using the deterministic model is in good agreement with the region of bistability determined using the stochastic model (Figure 2.12).

2.8 Acknowledgements

Chapter 2 contains material to be submitted as Longo D, Hoffmann A, Tsimring LS, Hasty J. Coherent activation of a synthetic mammalian gene network. *Syst Synth Biol.* The dissertation author was the primary investigator and author of this paper.

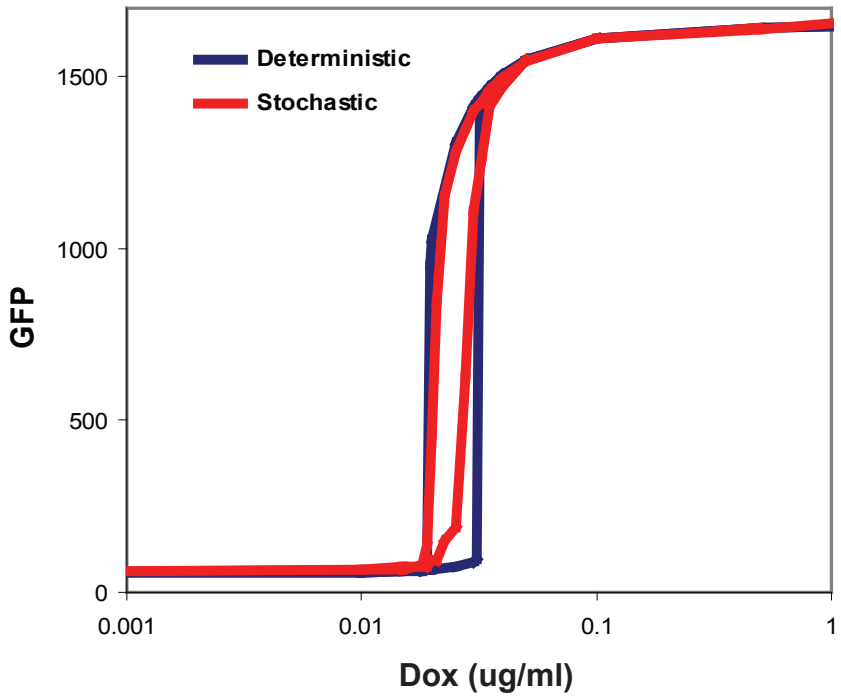

Figure 2.12: Steady-state dose response curves. Steady-state GFP expression levels versus dox concentration were determined using the deterministic model (blue) and the stochastic model (red). Steady-state GFP expression levels for the stochastic model were determined from 50 simulations for each dox concentration.

Table 2.1: Positive feedback circuit model variables

Variable	**Description**
m_A	rtTA mRNA levels
A	rtTA protein levels
P_A	promoter driving rtTA expression
m_G	GFP mRNA levels
G	GFP protein levels
P_G	promoter driving GFP expression

Table 2.2: Positive feedback circuit model reactions

Reaction	**Description**	**Rate coefficient**
$m_A \rightarrow \phi$	rtTA mRNA degradation	η_A
$m_A \rightarrow m_A + A$	rtTA translation	β_A
$A \rightarrow \phi$	rtTA protein degradation	δ_A
$P_A \rightarrow P + m_A$	rtTA transcription	$\frac{\alpha_A(1+f(AK_a)^n)}{1+(AK_a)^n}$
$m_G \rightarrow \phi$	GFP mRNA degradation	η_G
$m_G \rightarrow m_G + G$	GFP translation	β_G
$G \rightarrow \phi$	GFP protein degradation	δ_G
$P_A \rightarrow P + m_G$	GFP transcription	$\frac{\alpha_G(1+f(AK_a)^n)}{1+(AK_a)^n}$

Table 2.3: Positive feedback circuit model parameter values

Parameter	**Parameter Description**	**Value**
η_A (Raj *et al.*, 2006)	rtTA mRNA degradation rate	.18/hr
η_G (Raj *et al.*, 2006)	GFP mRNA degradation rate	.18/hr
δ_A	rtTA protein degradation rate	.03/hr
δ_G (Corish and Tyler-Smith, 1999)	GFP protein degradation rate	.03/hr
α_A	rtTA basal transcription rate	.1/hr
α_G	GFP basal transcription rate	.1/hr
β_A	rtTA translation rate	3/hr
β_G	GFP translation rate	3/hr
n (Kramer and Fussenegger, 2005)	Hill coefficient	2
f	fold-induction of transcription	30
K_s	Michaelis constant	.08
S	doxycycline concentration	0−1 μg/ml

Chapter 3

Dual delayed negative feedback model of NF-κB signaling

3.1 Introduction

Many important signal transduction pathways contain a negative feedback motif consisting of an activator that activates its own repressor. Activated repression is capable of generating oscillatory behavior (Tyson, et al., 2003) and has been observed to do so in biological systems such as the Hes1 regulatory protein which controls neuronal differentiation (Shimojo et al., 2008), the p53-Mdm2 system that mediates the DNA damage response (Lahav et al., 2004), and the NF-κB signaling network that governs the immune response and inflammation (Hoffmann et al., 2002; Nelson et al., 2004).

The role of activated repression is well understood in the context of transient signaling as functioning to limit the duration of the induced activity. Indeed, misregulation of the negative feedback mechanisms that control NF-κB and p53 has been shown to generate prolonged inflammatory or genotoxic stress responses, respectively, that lead to cell death or chronic disease (Vogel-

stein et al., 2000; Tergaonkar, 2006). Further, negative feedback can sensitize and speed-up responses to weak or transient input signals (Lahav et al., 2004) when compared to constitutive attenuation mechanisms.

In contrast, the physiological role of oscillatory behavior induced by persistent signaling has been characterized for a much smaller number of systems. Recent work has shown that, in the calcium stress pathway in yeast, the frequency of nuclear localization of a stress-response transcription factor can be modulated by the magnitude of the extracellular calcium concentration, and this frequency modulation results in a coordinated expression of target genes (Cai et al., 2008). In the NF-κB and p53 signaling systems, the function of oscillations is still unknown. Oscillations in p53 activity were proposed to represent a counting mechanism that quantizes the response, ensuring a robust but appropriate amount of activity for a specific degree of DNA damage (Ma et al., 2005). An alternate view was proposed in which oscillations of the p53-controlling ATM kinase activity allow for periodic sampling of the damaged DNA to track its repair and, if necessary, drive further p53 signaling to sustain the repair programs (Batchelor et al., 2008). Oscillations in NF-κB activity were proposed to determine which genes would be transcriptionally induced, thereby representing a temporal code that conveys information about the stimulus to gene promoters (Nelson et al., 2004). However, it is not clear whether or not the frequency encodes information in this systems as no differences in NF-κB target gene expression were observed between oscillating and non-oscillating genetic variants (Barken et al., 2005).

Recent work has demonstrated that oscillations in NF-κB activity can be generated by pulsatile stimulation with TNFα (Ashall et al., 2009). How-

ever, an analysis of the repeated activation of NF-κB that is driven by an oscillating signal provides little information about the role of oscillations that naturally arise with persistent stimulation. Thus, the role(s) of oscillations in NF-κB activity remains unclear and several questions are still unanswered: Do these oscillations convey information encoded in the frequency to downstream processes? Do they function to generate a periodically recurring phase of sensitivity to stimuli or regulatory crosstalk representing a potential "counting" mechanism? Do they "quantize" the output signal, thus specifying robust units of activity? Or, are the oscillations caused by persistent signaling simply a non-functional by-product of the requirement for the negative feedback architecture to enable sensitive, fast responses to transient stimuli?

Mathematical models comprised of a small number of equations have led to a greater understanding of biological processes in terms of molecular interactions, diffusion, dose responses, gradient sensing, the role stochasticity in gene expression and in fate decisions (Lander et al., 2002; Kruse et al., 2004; Arkin et al., 1998; Aurell et al., 2002). Although several models of networks with autoregulation have been developed (Lipshtat et al., 2005; Ramsey et al., 2006; Kim et al., 2007), most of these networks do not incorporate delays. In signaling, however, such elegant models often do not faithfully reproduce the dynamic behavior of the signaling system because actual biological networks involve many molecular interactions that tend to slow overall signal processing. Larger models comprised of many molecular species and parameters have proven useful in exploring dynamic signaling behavior via computational simulations in conjunction with experimental studies, but they are analytically intractable and therefore do not provide the degree of conceptual insights that

small models do.

Here we pursue an alternative approach to modeling NF-κB signaling. We construct a new model that replaces cascading reactions with a single but delayed compound reaction that enables both recapitulation of experimentally observed dynamics and the use of powerful analytical tools. With these tools, we explore the physiological function of the dynamic behavior of NF-κB produced by the activated repression mechanism mediated by its inducible inhibitors, IκBα and IκBϵ. The mathematical analysis results in predictions that are addressed experimentally and thus lead to fundamental insights about the function and origins of this signaling system.

3.2 NF-κB model with a single delayed negative feedback loop

The basic structure of the NF-κB signaling module is shown in Figure 3.1A. In resting cells, NF-κB is sequestered in the cytoplasm by IκB proteins. Cellular stimulation leads to activation of the IκB kinase (IKK) which phosphorylates IκB proteins thus targeting them for degradation. Upon degradation of IκB proteins, NF-κB moves into the nucleus and activates hundreds of target genes including the predominant IκB isoform, IκBα. Synthesized IκBα enters the nucleus, binds to NF-κB, and the IκBα-NF-κB complex is exported back to the cytoplasm. Thus, the core feature of the NF-κB signaling module is a negative feedback loop mediated by IκBα. This can be abstracted to a simple motif in which x (NF-κB) activates y (IκBα), y represses x, and repression of x by y is relieved by K (IKK) (Figure 3.1B).

Using this motif as a guide, we formulated our model of the IκBα-

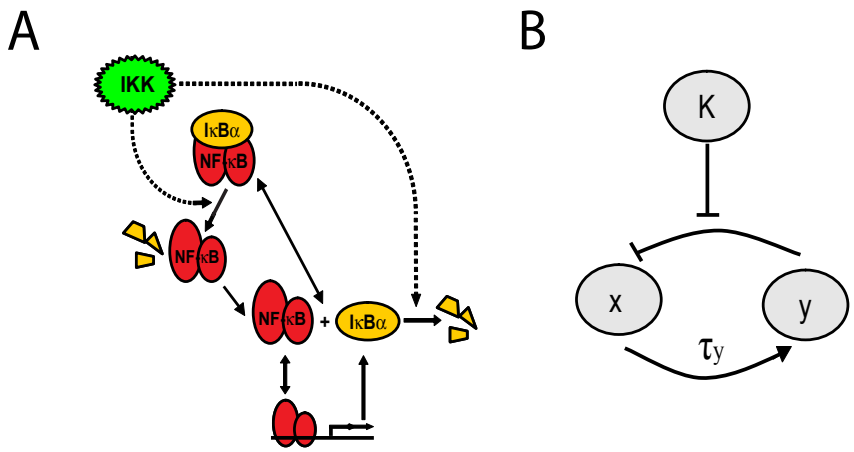

Figure 3.1: Single negative feedback loop system. (A) Diagram of the IκBα-NF-κB signaling module. (B) Diagram of a system with a single delayed negative feedback loop.

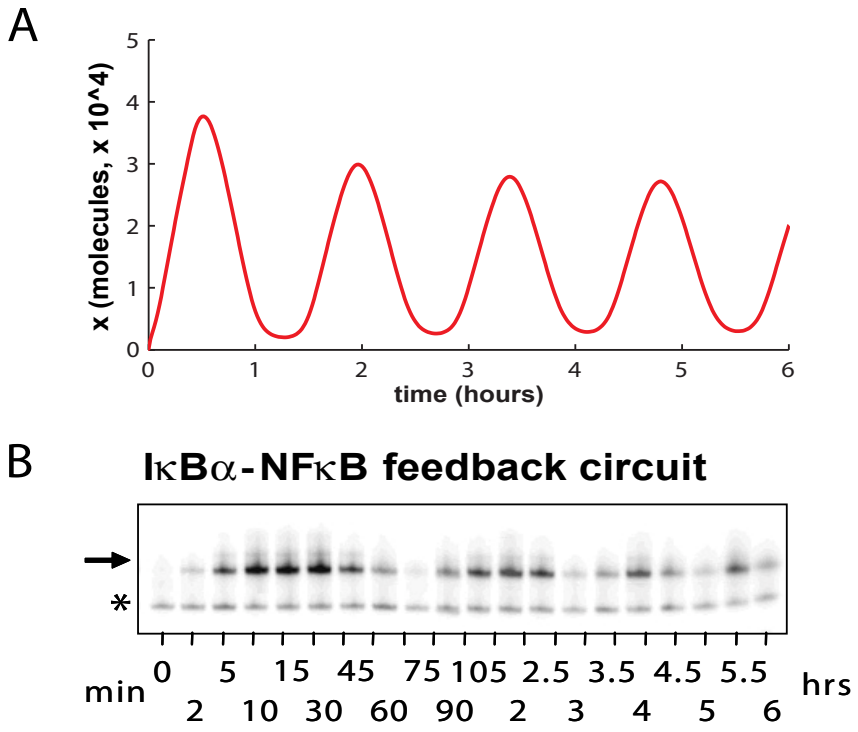

Figure 3.2: Pronounced oscillations in nuclear NF-κB levels for a system with a single IκBα-mediated negative feedback loop. (A) Nuclear NF-κB levels (x) in response to persistent stimulation as a function of time produced using our delayed feedback model. (B) Experimental levels of nuclear NF-κB (determined by EMSAs) in cells with only the IκBα-mediated negative feedback loop intact (reproduced from Hoffmann et al., 2002, Figure 2A). The arrow indicates specific nuclear NF-κB binding and the asterisk indicates nonspecific DNA binding.

mediated NF-κB response as a set of 9 reactions (Tables 3.1A, 3.2A). Specifically, the model assumes that the total number of the NF-κB molecules (X) is conserved, however they can exist either in free/nuclear form (x) or sequestered outside of nucleus within the IκBα-NF-κB complex ($[xy]$). The model contains non-delayed reactions for the binding of free NF-κB to the unbound IκBα promoter (d_{0y}) to form the bound IκBα promoter (d_{1y}), binding of IκBα protein (y) to free NF-κB to form the IκBα-NF-κB complex, constitutive degradation of IκBα, and induced degradation of free and bound IκBα proteins by the IκB kinase IKK (K) producing free NF-κB. In contrast, a compound delayed reaction describes the synthesis of IκBα protein. This reaction involves a time delay τ_y, which represents the time needed for transcription, translation, nuclear import and export, and protein-protein interactions.

Using experimentally validated assumptions (see Materials and Methods), we reduced the set of mass-action kinetics equations for the 9 reactions to a single delay-differential equation:

$$Y'_y \dot{y} = a_y d_{0y}(y_\tau) + b_y d_{1y}(y_\tau) - g_y y - K r_y Y(y) \tag{3.1}$$

where $Y(y) = y[1 + c_y X/(1 + c_y y)]$ is the total IκBα concentration (the sum of free IκBα (y) and IκBα bound to NF-κB), $d_{0y}(y) = F d_y/[F + X/(1 + c_y y)]$, $d_{1y}(y) = X d_y/[F(1 + c_y y) + X]$, are the probabilities for the IκBα promoter to be free or bound to NF-κB, respectively, $F = f_1/f_0$, $c_y = k_y/(k_{-y} + K r_y)$, and the subscript τ denotes the variable taken at time $t - \tau_y$. The rates of individual reactions $k_y, k_{-y}, f_1, f_0, c_y, g_y, r_y, a_y$ are defined in Table 3.2.

Mirroring the biological system, the IKK variable, $K(t)$, is used as the input signal. The first term in the r.h.s. of Eq. 3.1 represents constitutive

synthesis from the unbound IκBα promoter, the second term represents induced synthesis from the NF-κB-bound IκBα promoter, the third term represents constitutive degradation of IκBα protein, and the fourth term represents IKK-induced degradation of IκBα. Nuclear NF-κB level x at any time can be determined directly from IκBα levels via $x = X/(1 + c_y y)$. The time delay τ_y is incorporated in the synthesis terms: we assume that the rate of production of new proteins at time t depends on the state of the system at time $t - \tau_y$. Any of the time-dependent parameters entering production terms should also be taken at time $t - \tau_y$. Incorporating this time delay allows us to explore the behavior of the negative feedback loop without simulating the full set of reactions associated with it. We obtained values for the time delay and for the other model parameters by calibrating the behavior of the model with experimental results (Table 3.3). As a starting point, we used parameter values from biochemical measurements (Kearns et al., 2006). However, some modifications were necessary because these values represent the rates of single reaction steps and the model contains compound reactions.

To validate the model, we compared it to experiments. In response to a persistent IKK input signal (starting at time $t = 0$), our simulations of the IκBα-mediated negative feedback system show pronounced oscillations in nuclear NF-κB levels with an oscillation period of about 90 minutes (Figure 3.2A). Oscillations with a similar period were observed experimentally when mutant cells containing only the IκBα feedback loop were persistently stimulated with the inflammatory cytokine TNF (Figure 3.2B).

3.3 Linear stability analysis of a single-feedback loop system

The advantage of our modeling approach is that it allows for analytical studies of the network dynamics. Here, we perform a linear stability analysis of the delay-differential equation (Eq. 3.1) to identify the characteristic period and decay rate of NF-κB oscillations produced when IKK signal is present ($K > 0$). For sufficiently large K, induced synthesis and degradation are much stronger than basal ones, so the latter can be neglected ($a_y = g_y = 0$).

Expressing y via Y and substituting it into d_{0y}, d_{1y} yields a closed equation for Y in the form

$$\dot{Y} = G(Y_\tau) - Kr_y Y \tag{3.2}$$

where $Y_\tau = Y(t - \tau_y)$ and the function $G(\cdot)$ has the form

$$G(Y) = d_y \frac{b_y c_y (X - Y) - b_y + b_y \sqrt{(c_y(X - Y) - 1)^2 + 4c_y X}}{2c_y F + c_y(X - Y) - 1 + \sqrt{(c_y(X - Y) - 1)^2 + 4c_y X}} \tag{3.3}$$

The fixed point Y_s (stationary solution) of this equation is given by the algebraic equation

$$G(Y_s) = Kr_y Y_s \tag{3.4}$$

and the stability of this solution is determined by the linearized equation for a small perturbation ξ near Y_s,

$$\dot{\xi} = B\xi_\tau - Kr_y \xi \tag{3.5}$$

where $\xi = Y - Y_s$, $B = dG(Y_s)/dY$ is the Jacobian whose explicit expression is given in the Materials and Methods, and the subscript τ again indicates the delayed value of ξ taken at time $t - \tau_y$.

The eigenvalue λ can be found by substituting $\xi = \xi_0 \exp(\lambda t)$, yielding the transcendental equation

$$\lambda = Be^{-\lambda t} - Kr_y \tag{3.6}$$

which has a complex solution in terms of the Lambert function $W(z)$ defined via $We^W = z$,

$$\lambda = \tau_y^{-1} W(B\tau_y e^{Kr_y\tau_y}) - Kr_y \tag{3.7}$$

The imaginary part of λ gives the oscillation frequency $\omega = 2\pi f$, and the (negative) real part of λ gives the decay rate δ of oscillations. Plotting the period ($T = 1/f$) (Figure 3.3A) and decay (δ) (Figure 3.3B) of the oscillations as a function of the delay reveals a strong dependence. In contrast, the signaling perturbation K (the IKK kinase) that acts as the input for the model determines the amplitude of the response but only negligibly affects the period or the oscillation decay (Figure 3.3). Thus, we find that the period is highly dependent on the delay but is rather insensitive to changes in the input level. This is confirmed by direct simulations of the full nonlinear equation (Eq. 3.1), where time series of x are plotted for several different values of τ_y and K (Figure 3.4). Since variations of stimulus do not lead to significant frequency modulation of NF-κB activity, oscillations of NF-κB are unlikely to encode information about the stimulus. Therefore, we believe that the oscillations generated in the single feedback loop NF-κB module, are the unintended byproduct of the regulatory activity of the negative feedback subsystem. We will return to this issue below.

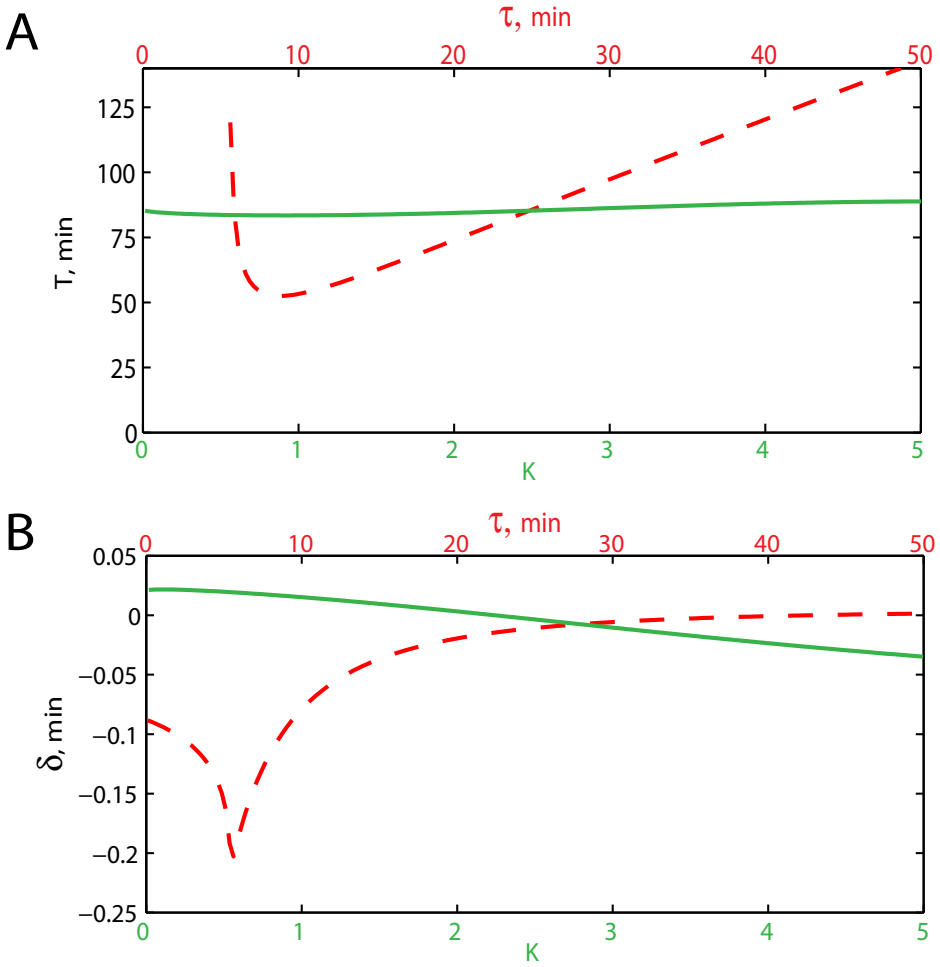

Figure 3.3: Analysis of the characteristic period and the decay rate of oscillations produced by the IκBα-mediated negative feedback loop. (A) The oscillation period T as a function of K with $\tau_y = 25$ min (green line) and as a function of τ_y with $K = 2$ (red dashed line). (B) The oscillation decay rate δ as a function of K with $\tau_y = 25$ min (green line) and as a function of τ_y with $K = 2$ (red dashed line). Work done by colleague Lev Tsimring.

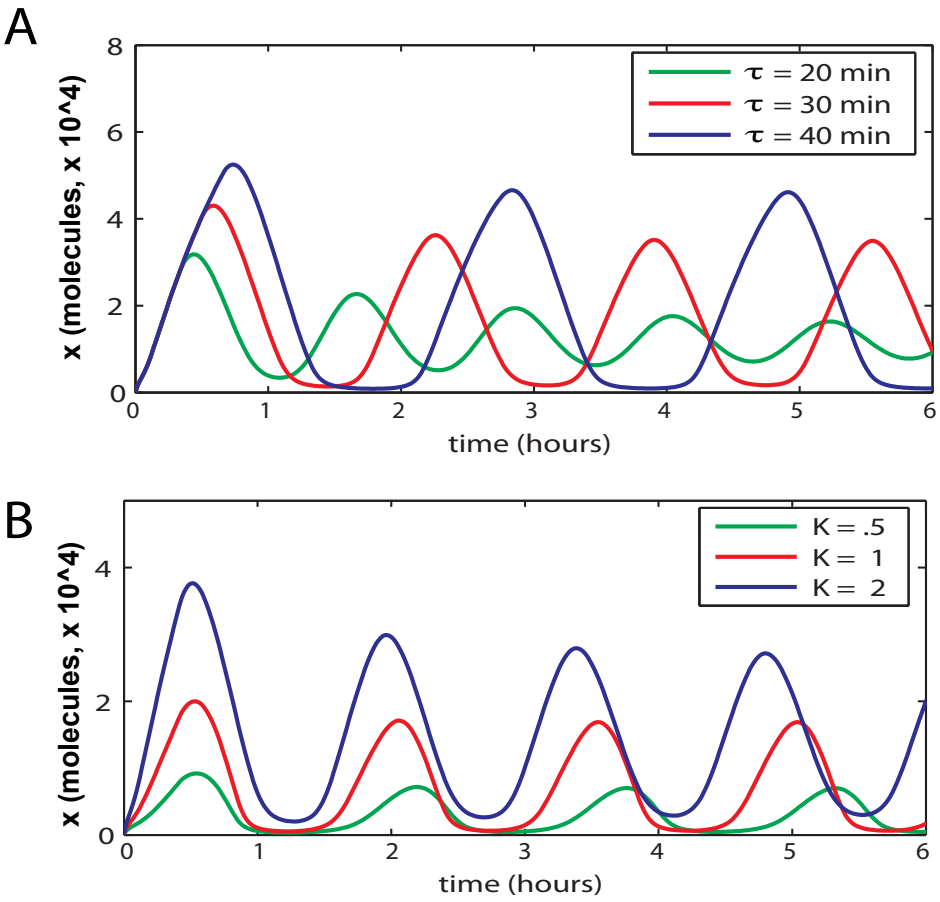

Figure 3.4: Time series of x for several values of τ_y and K. Oscillations produced by the IκBα-mediated negative feedback system with (A) $K = 2$ for $\tau_y = 20$ min, $\tau_y = 30$ min, and $\tau_y = 40$ min and with (B) $\tau_y = 25$ min for $K = .5$, $K = 1$, and $K = 2$.

3.4 Damping of oscillations in a dual delayed feedback loop system

It is well known that the wild-type NF-κB system does not exhibit significant oscillations in response to persistent stimuli. The main qualitative difference between the one-loop system considered in the previous section, and the wild-type NF-κB module is the presence of another IκB isoform, IκBϵ, which also provides negative feedback regulation on NF-κB activity (Figure 3.5A, B), however with slower kinetics (Kearns et al., 2006). Experimental and computational work has shown that IκBϵ-mediated feedback can cause damping of IκBα-mediated oscillations (Kearns et al., 2006) and (Figure 3.6A). More recent computational work has predicted that IκBϵ-mediated feedback desynchronizes oscillations but does not dampen oscillations in single cells (Ashall et al., 2009). Thus, the mechanism by which IκBϵ-mediated feedback produces damped oscillations at the population level is not well established. Furthermore, it is unknown whether the damping function of the IκBϵ-mediated feedback loop has evolved to achieve a specific regulatory function or may simply be a secondary consequence of another function. We hypothesize that the main role of the second feedback loop is to mitigate the undesirable oscillations produced by the first feedback loop. To test this hypothesis, we expanded the model to include an additional 9 reactions involving IκBϵ (Tables 3.1B, 3.2B). Following the same reduction procedure (see Materials and Methods), we derived a deterministic model consisting of two coupled delay-differential equations for the concentrations of the two IκB isoforms, IκBα (y) and IκBϵ

(z),

$$\dot{Y} = a_y d_{0y}(y_\tau, z_\tau) + b_y d_{1y}(y_\tau, z_\tau) - g_y y - K r_y Y \tag{3.8}$$

$$\dot{Z} = m\left[a_z d_{0z}(y_\tau, z_\tau) + b_z d_{1z}(y_\tau, z_\tau)\right] - g_z z - K r_y Z \tag{3.9}$$

where $Y = y[1 + c_y X/(1 + c_y y + c_z z)]$, $Z = z[1 + c_z X/(1 + c_y y + c_z z)]$, $d_{0y,0z} = F d_{y,z}/(F+x)$, $d_{1y,1z} = x d_{y,z}/[F+x]$, $x = X/(1+c_y y+c_z z)$, $c_{y,z} = k_{y,z}/(k_{-y,-z}+ K r_{y,z})$, and $y_\tau = y(t - \tau_y)$, $z_\tau = z(t - \tau_z)$. Parameter $0 < m < 1$ here is the scaling factor which characterizes the relative strength of the secondary feedback loop.

In Eqs. 3.8 and 3.9, Y represents total IκBα (the sum of free IκBα (y) and IκBα bound to NF-κB $([xy])$, and Z represents total IκBϵ (the sum of free IκBϵ (z) and IκBϵ bound to NF-κB $([xz])$). The terms in the r.h.s. of Eqs. 3.8 and 3.9 again represent constitutive synthesis from the identical unbound IκBα and IκBϵ promoters, induced synthesis from the NF-κB-bound promoters, constitutive degradation of IκBα and IκBϵ proteins, and IKK-induced degradation of IκBα and IκBϵ. Nuclear NF-κB levels are determined directly by IκBα and IκBϵ levels. Parameter values for the IκBα-mediated reactions were determined in the previous section. For the IκBϵ feedback reactions, we use the same parameter values except for the constitutive synthesis and the constitutive degradation rates, which were chosen based on experimental measurements (Kearns et al., 2006) (Table 3.3).

To address our hypothesis that IκBϵ-mediated feedback specifically evolved to dampen IκBα-mediated oscillations, we performed a parameter optimization procedure to determine the IκBϵ synthesis parameters that result in maximum damping. To characterize the degree of damping, we chose the

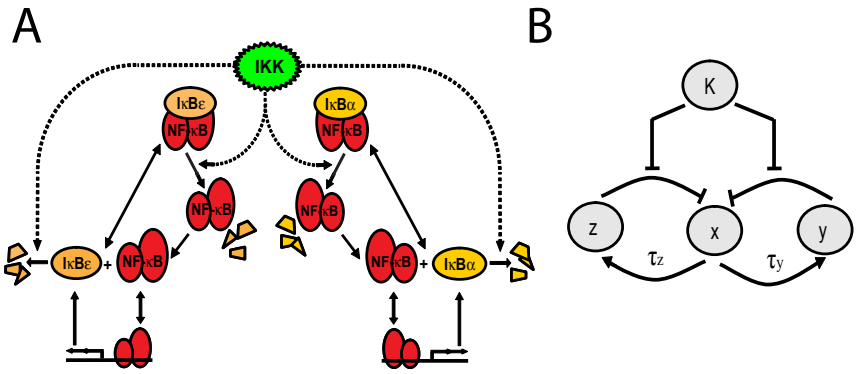

Figure 3.5: Dual negative feedback system. (A) Diagram of the system with both IκBα- and IκBϵ-mediated feedback. (B) Diagram of a system with dual delayed negative feedback loops.

maximum peak-trough difference after 6 hrs as a metric for the persistence of oscillations. According to the definition of this performance metric, "optimal damping" occurs when this metric is minimized. In our optimization procedure, we varied two important parameters, the time delay of the second feedback loop τ_z and the scaling factor m which simultaneously varies the rates of constitutive and induced synthesis of IκBϵ. Choosing $m = 0$ is equivalent to the complete removal of the IκBϵ-mediated negative feedback loop while $m = 1$ represents the case in which the inducible synthesis rates for IκBϵ are the same as for IκBα. The two-dimensional optimization search is shown in a color map (Figure 3.6B) indicating that the performance metric is minimized at $m = 0.3, \tau_z = 72$. Time course simulations with the optimized parameter set show a high degree of damping (Figure 3.6E) similar to what is observed experimentally (Figure 3.6A).

To determine whether these optimized parameter values correspond to observations, we measured relevant parameter values experimentally. The synthesis delays for IκBα and IκBϵ were determined by measuring IκBα and IκBϵ mRNA levels in a time course of TNF-treated murine embryonic fibroblasts (MEFs) in multiple independent experiments (Figure 3.6E, 3.7A, B). The measured delay for IκBα was 25.8$\pm$5.4 min, and 59.4$\pm$12.8 min for IκBϵ, which agrees well with the model prediction for optimal damping.

Since it is difficult to measure the promoter strength experimentally, we employed an implicit way of comparing experiment with the model. To relate the parameter value m to experimental measurements, we set $m = 0.3$ in the model and calculated the ratio of peak values for IκBα and IκBϵ proteins R_m, which we found to be equal to 3.9. Then we measured the ratios of

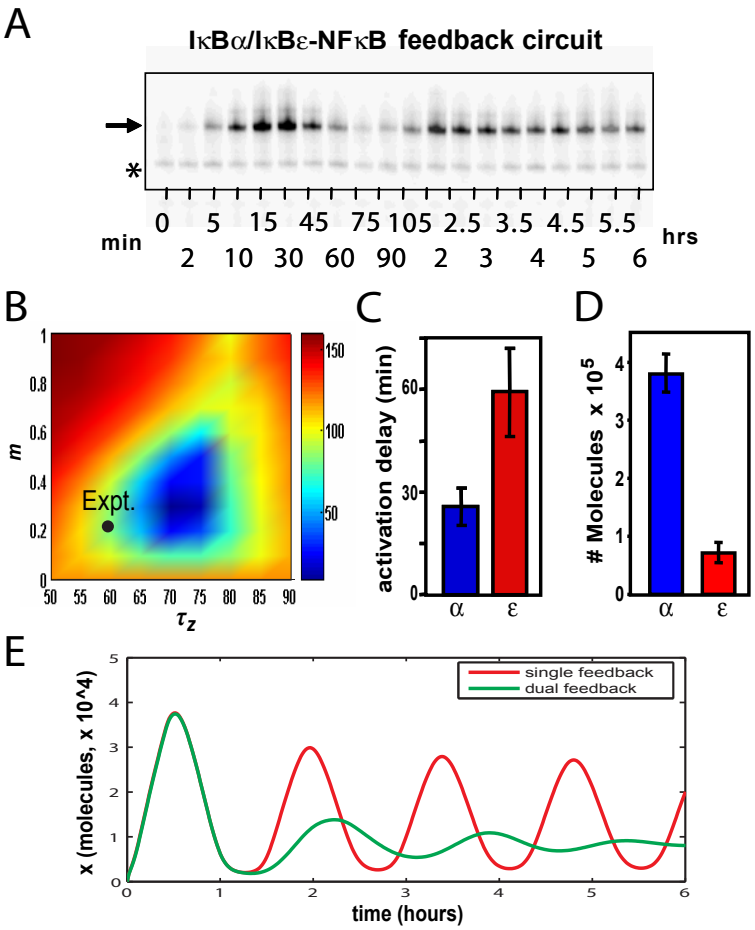

Figure 3.6: Damped oscillations with dual negative feedback. (A) Experimental levels of nuclear NF-κB (determined by EMSAs) in wild-type cells containing both IκBα- and IκBϵ-mediated negative feedback (reproduced from Hoffmann et al., 2002, Figure 2E). The arrow indicates specific nuclear NF-κB binding and the asterisk indicates nonspecific DNA binding. (B) Optimization of the parameters of the second feedback loop m and τ_z towards maximizing the oscillations damping. The global minimum occurs at $\tau_z = 72$ min, $m = .3$. The black dot indicates the experimentally measured parameter values ($\tau_z = 59$ min, $m = .2$). The value of m corresponding to the experimentally measured value of R_e was determined with the model (see Figure 3.8). (C) Experimental measurements of IκBα and IκBϵ synthesis delays. (D) Experimental values for peak IκBα and IκBϵ protein levels. (E) Simulated time course of nuclear NF-κB levels (x) for the single feedback system and for the optimized dual feedback system in response to persistent stimulation with $K = 2$. Experimental work done by colleague Jeff Kearns.

basal (unstimulated) to peak protein levels for IκBα and IκBϵ in experiment via quantitative Western blots of whole cell lysates generated during a TNF time course. These were compared to recombinant protein standards to derive absolute molecule number per cell. Peak IκBα protein levels were measured to be 379,800 molecules per cell, and IκBϵ 71,300 molecules per cell, with both values being subject to an estimated 25% error (Figure 3.7C, D). These protein levels correspond to the experimental peak values ratio $R_e = 5.3$ which is close to the model prediction $R_m = 3.9$.

We believe that it is unlikely that such a good correspondence between model prediction for optimal damping and naturally occurring values of relevant parameters can be a simple coincidence. In our opinion, these results suggest that the NF-κB signaling module in mammalian cells may indeed have evolved a second delayed negative feedback loop mediated by IκBϵ to dampen the oscillatory propensity of the IκBα negative feedback loop.

3.5 Fine temporal control with a dual feedback loop system

Given that the main function of the secondary negative feedback loop in the NF-κB signaling module appears to be the dampening of oscillations produced by the primary feedback loop, the question remains as to what function of the strong primary negative feedback loop led to its selection despite these unwanted oscillations. Our hypothesis is that the primary negative feedback loop is needed to produce a strong rapid response to an external stimulus, which would be turned off quickly and efficiently after the signal is terminated. To evaluate this hypothesis, we first simulated persistent stimulation of a vari-

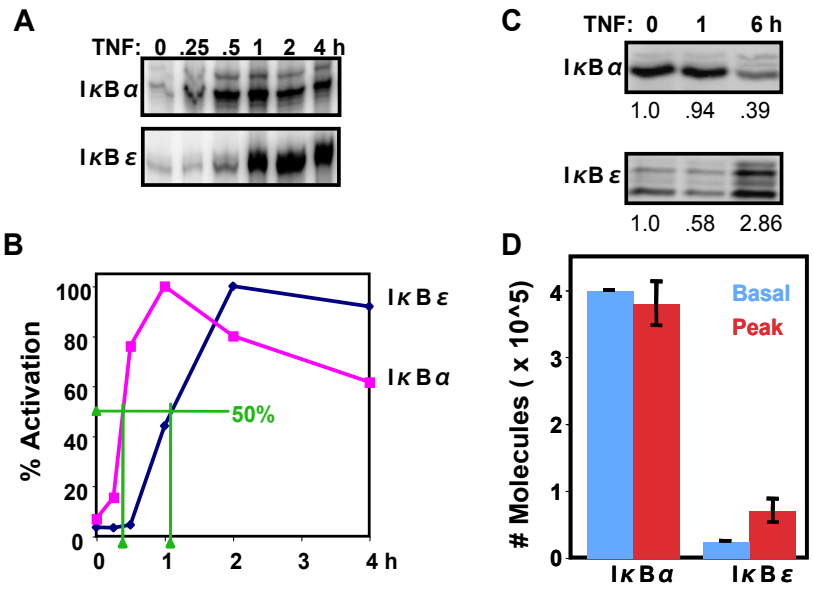

Figure 3.7: Representative experimental data for IκBα and IκBϵ synthesis delays and feedback strengths. (A) mRNA synthesis for IκBα and IκBϵ were measured by RNase Protection Assay in wild-type immortalized MEF cells in response to 10ng/mL TNF chronic stimulation. (B) The RPA results were quantitated to determine the intensity of each band in the gel (ImageQuant, GE Healthcare). The highest intensity band in each set was set to 100% Activation and the other bands were normalized accordingly. The delay time to reach half maximal synthesis was calculated as the time at which the activation curve crossed the 50% level. A set of N=10 replicate experiments were performed to calculate the global average. (C) The protein abundances for IκBα and IκBϵ at their respective activation peaks in wild-type immortalized MEF cells chronically stimulated with 10ng/mL TNF were measured by Western Blot analysis (IκBα at 1 h and IκBϵ at 6 h) . Fold induction vs. basal state are shown below each gel and were calculated by quantitation of the band intensities and normalization to the 0 h band. (D) Bar plot of the average protein abundances from multiple Western Blot experiments for peak levels of IκBα (N=7) and IκBα (N=5). The basal state abundances were measured by comparison to a standard curve of recombinant IκBα or IκBϵ protein (JD Kearns, S Basak, C Lynch, A Hoffmann *in preparation*). Peak abundances were calculated by multiplying the quantitated fold induction (as in C) by the basal abundance. Error bars on the peak bars represent one standard deviation. Work done by colleague Jeff Kearns.

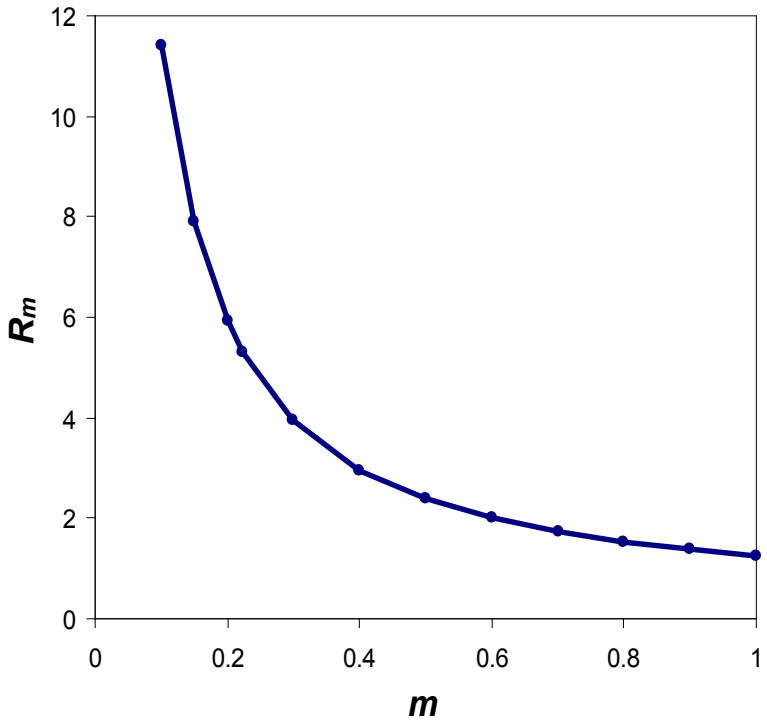

Figure 3.8: Plot of R_m as a function of m. The ratio of peak IκBα protein levels to peak IκBϵ protein levels (R_m) was determined for several values of m in the model simulations to determine the value of m corresponding to $R_m = 5.3$ (The experimentally measured value for the ratio is $R_e = 5.3$). This value of m ($m = .2$) was used to plot the point in Figure 3.6B which indicates the experimental values of m and τ_z.

ant of NF-κB system without feedback (we assume that IκBα is constitutively produced, so $d_{0y} = 1, d_{1y} = 0$ in Eq. 3.1) and found that this system produces long term, non-oscillatory NF-κB activity (Figure 3.9 *Top, blue line*). Motivated by the fact that within the physiological setting TNF is secreted in bursts and therefore perceived by surrounding cells as transient or pulse stimulation, we then performed pulse stimulations of 15, 30, and 45 min in duration. In this system, the pulses resulted in a transient response that was attenuated very slowly. Faster attenuation can be achieved by increasing the constitutive synthesis rate, a_y. Increasing a_y by two orders of magnitude results in pulse NF-κB responses to transient stimuli, but the responsiveness (in amplitude) is much reduced (Figure 3.11).

We then performed similar simulations in a single negative feedback loop NF-κB system and found that this network topology allows for a rapid shutdown of NF-κB activity for transient inputs (Figure 3.9 *Middle*). This suggests that the NF-κB network may have evolved from a pathway without feedback to a pathway with a single negative feedback loop to allow for a more sensitive transient response. Although the negative feedback indeed allows for greater sensitivity, a side effect of having negative feedback is that pronounced oscillations arise when the input signal persists for a long time period (Figure 3.9 *Middle*). The addition of a second negative feedback loop with a different time delay can help to dampen these oscillations, while preserving the responsiveness of the signaling module to transient stimuli (Figure 3.9 *Bottom*).

By plotting the duration of the response (above a given threshold) we investigated what may be called "temporal dose response curves" of the single and dual feedback systems (Figure 3.10). The dual feedback system has a

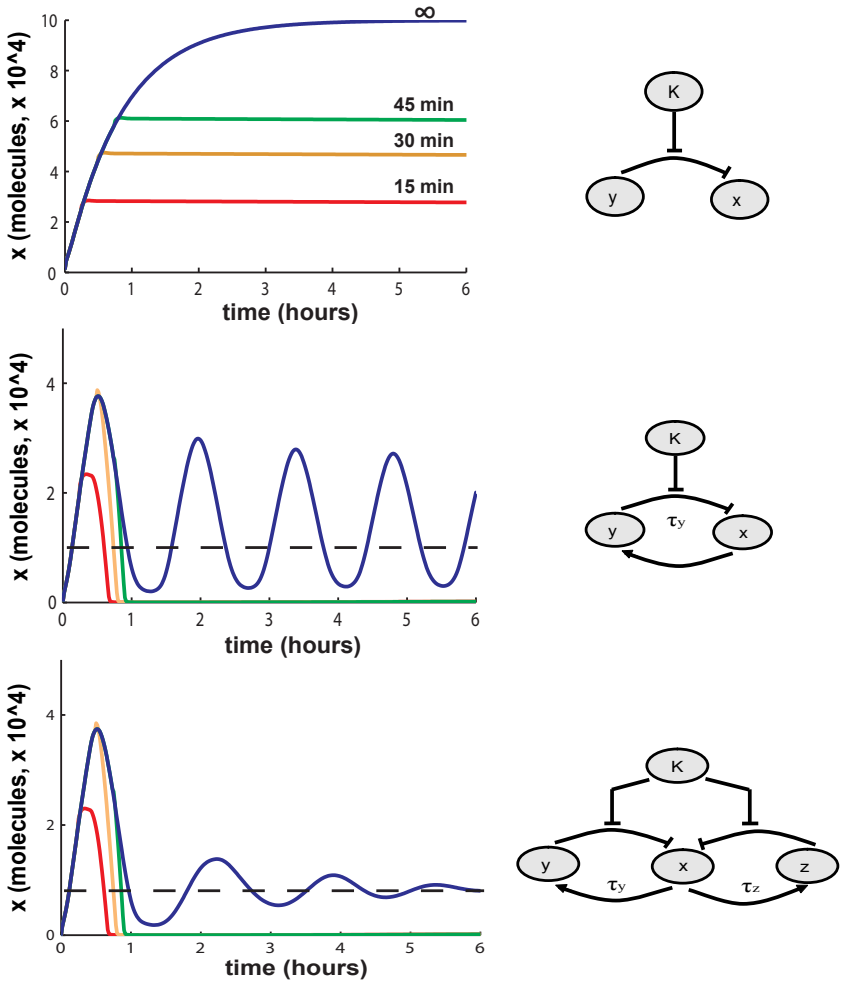

Figure 3.9: Response of the NF-κB signaling module to transient stimulation with magnitude $K = 2$. Time series of x for a system with all feedback removed (top), a system with IκBα-mediated negative feedback (middle), and a system with both IκBα- and IκBϵ-mediated negative feedback (bottom) in response to 15 min (red), 30 min (orange), 45 min (green), and persistent (blue) stimulation.

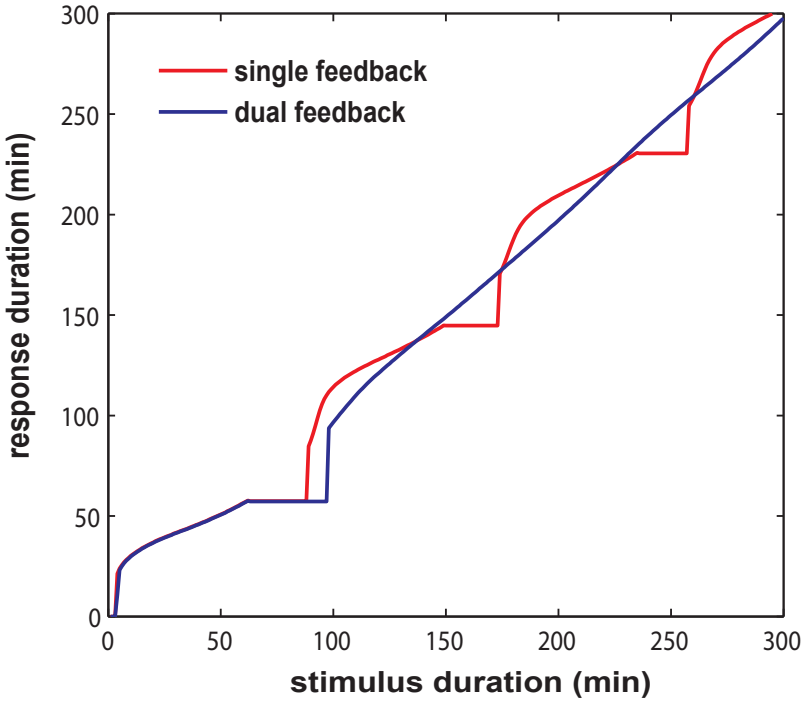

Figure 3.10: Temporal dose response curves. The response duration is plotted as a function of the stimulus duration for the single feedback and dual feedback systems. The response duration is the amount of time x exceeds a threshold level of 50 (as indicated by the dashed black lines in the graphs shown in Figure 3.9.)

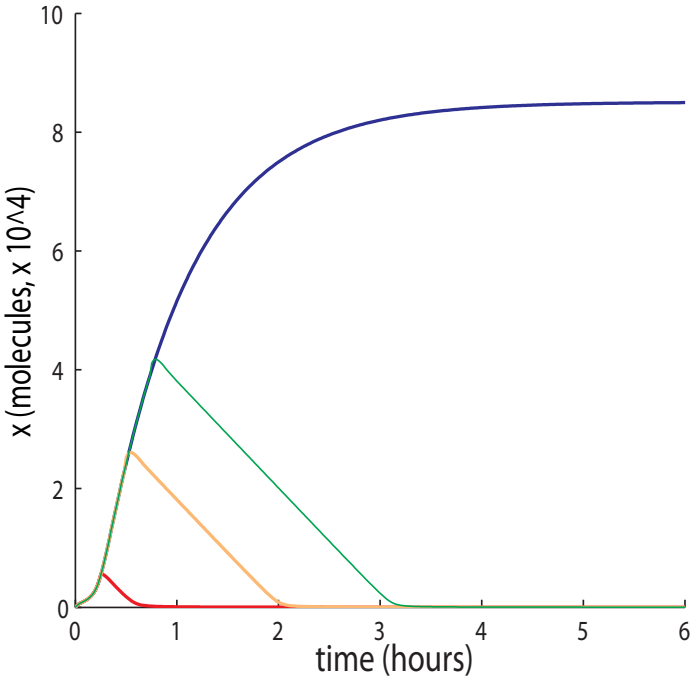

Figure 3.11: Response of a no-feedback system with constitutive IκBα synthesis (a_y) increased from 0.00185 nM/min to 0.3 nM/min. The time series of x is shown for 15 min (red), 30 min (orange), 45 min (green), and persistent (blue) stimulation.

response duration close to 60 min for short pulses (< 100 min), and a duration proportional to the input duration for longer pulses. The single feedback system has the same behavior as the dual feedback system for short inputs, but for longer inputs the single feedback system produces a quantized response with the same output duration for several different input durations. Our analysis indicates that a dual feedback system is able to produce temporally graded responses, whereas a single feedback system that oscillates does not. Given that the duration of the second phase of the NF-κB response to TNF is a critical determinant of gene expression programs (Hoffmann et al., 2002), we suggest that the NF-κB system has evolved a dual feedback system that allows for NF-κB activity whose duration is more closely related to the duration of the cytokine stimulus.

This fine temporal control, achieved via dual negative feedback, may be critical for the cell-to-cell interactions involved in the adaptive immune response present in vertebrates, but may not be necessary for innate immune responses. We hypothesize that, on an evolutionary timescale, the appearance of dual negative feedback loops that regulate NF-κB activity coincides with the transition from an innate to an adaptive immune system. To address this hypothesis, we used BLASTP with an E-value cutoff of 1e-25 to search for homologs of the mouse IκBα and IκBϵ protein sequences in other organisms (see Materials and Methods). We found homologs for both IκBα and IκBϵ, not only in other mammals (such as chimp, dog, platypus), but also in other vertebrate classes including fish, amphibians, and birds (Figure 3.12, Materials and Methods). Thus, dual negative feedback regulation of NF-κB activity appears to be present in all organisms with adaptive immunity. In contrast,

we did not find any invertebrate organisms with homologs for both IκBα and IκBϵ (Figure 3.9, Materials and Methods). Therefore, invertebrates, which lack adaptive immunity, also appear to lack the potential for dual negative feedback regulation of NF-κB mediated by IκBα and IκBϵ suggesting that the temporal control achieved with this regulatory architecture is not necessary for innate immune responses.

3.6 Additional role of negative feedback: Robustness to fluctuations

Thus far, we have examined the response of the network to transient IKK signals in the absence of fluctuations. However, it is well known that noise in gene expression can cause significant variability in cellular responses (Thattai and van Oudenaarden, 2001; Swain et al., 2002; Elowitz et al., 2002; Rosenfeld et al., 2005; Lipshtat et al., 2005; Volfson et al., 2006). Sometimes this variability can be beneficial (Hasty et al., 2000), but in most cases, noise has a detrimental effect on the robustness of cellular functions. Mechanisms have presumably evolved to mitigate the unwanted effects of noise, especially in signaling pathways. In this section we examine the variability in the response of the NF-κB module that arises due to intrinsic and extrinsic noise, and we demonstrate that the dual-feedback loop architecture allows for a more robust response than the single feedback loop system. Further, we investigate how the relative contribution of intrinsic and extrinsic fluctuations depends on the size of the system.

The concentration of signaling molecules such as NF-κB can vary significantly between cells (Dower and Qwarnstrom, 2003). This variability in

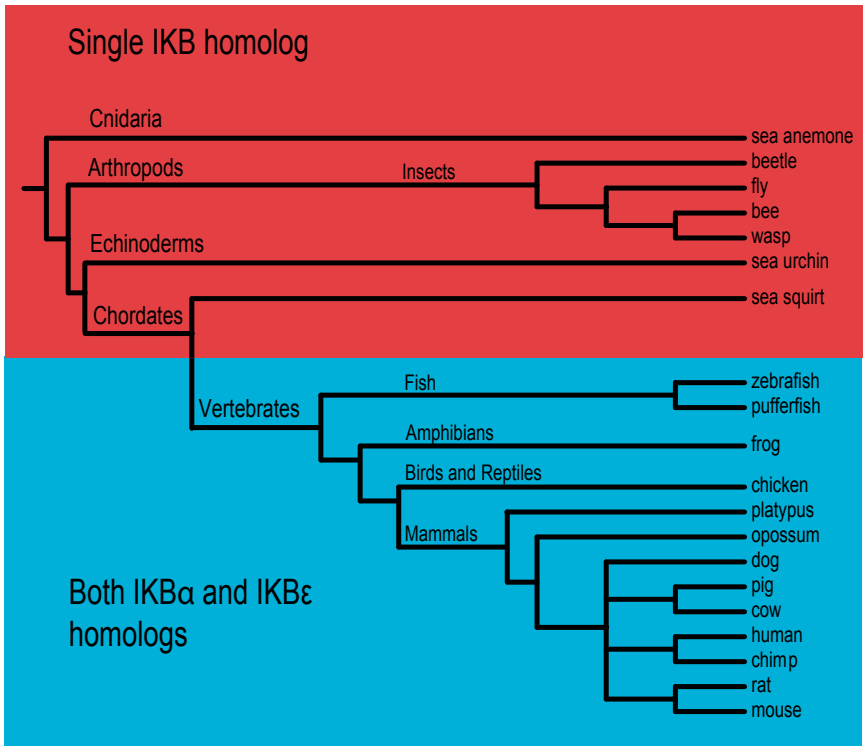

Figure 3.12: Schematic of a phylogenetic tree showing organisms in which homologs for IκBα and IκBϵ were found using BLASTP. Organisms in which both IκBα and IκBϵ were found (in blue) and organisms in which a single homolog was found (in red) using BLASTP. The branches in the schematic phylogenetic tree are not drawn to scale. (For simplicity, not all organisms with single or dual homologs are shown here. A complete list is provided in the Materials and Methods).

protein levels represents a source of extrinsic noise. We examined the variability in the response of the network to fluctuations in the total level of NF-κB and fluctuations in the IKK input level by simulating the network behavior with total NF-κB levels and IKK levels altered by up to $\pm 50\%$. The coefficient of variation (CV) in peak nuclear NF-κB levels and the CV in late-phase nuclear NF-κB levels is defined as $CV = 2(x_{max} - x_{min})/(x_{max} + x_{min})$ where x_{max} (x_{min}) are the maximum (minimum) values of NF-κB at the peak or during the late-phase. We find that the CV in peak nuclear NF-κB increases linearly with extrinsic variation in total NF-κB and with extrinsic variation in IKK with identical CV values for both the single and dual feedback models (Figure 3.13*A,B*). In contrast, the CV in late-phase (asymptotic) NF-κB levels are significantly lower in the dual feedback system than in the single feedback system. The CV in late-phase NF-κB for the dual feedback system increases linearly from 0 to approximately 1 as the range of total NF-κB (Figure 3.13*C*) and IKK (Figure 3.13*D*) is increased to $\pm 50\%$, while the CV in late-phase NF-κB for the single feedback system increases from approximately 1.6 to 1.9 (Figure 3.13*C,D*). Thus, in the presence of extrinsic variations in IKK and total NF-κB, the dual feedback system allows for a late-phase response which is more robust than the response produced by the single feedback system.

Intrinsic noise arises from the stochastic nature of biochemical processes such as transcription and translation (Elowitz et al., 2002). To examine the response of the NF-κB signaling module in the presence of intrinsic genetic noise, we used the Gillespie algorithm (Gillespie, 1977) modified according to (Bratsun et al., 2005) to perform stochastic simulations of both regular and delayed biochemical reactions included in our delayed feedback model. These

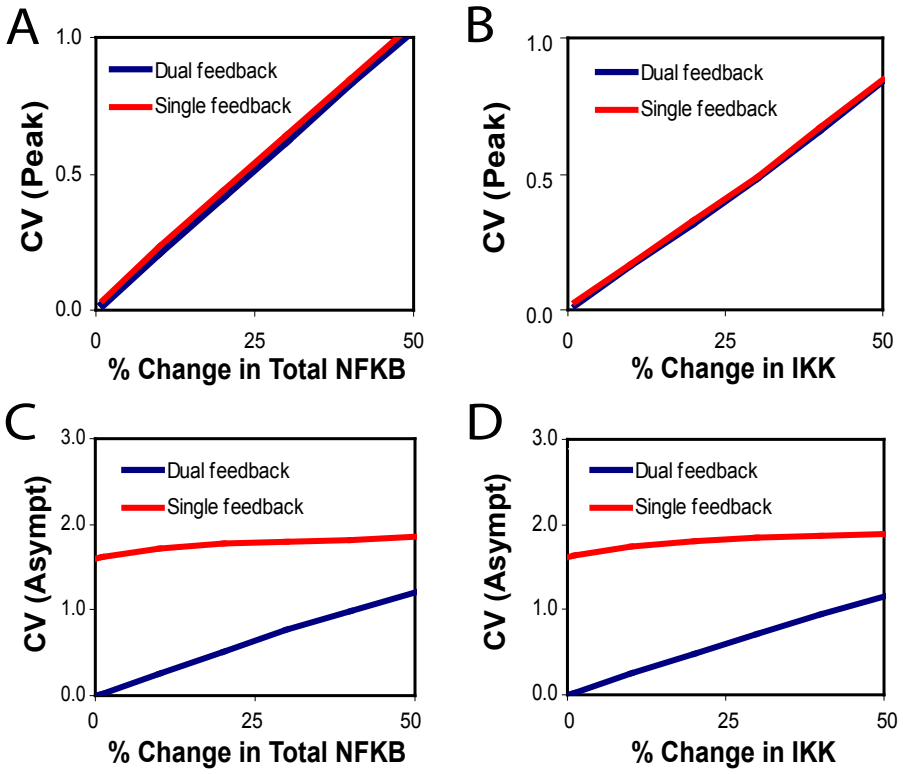

Figure 3.13: CV due to extrinsic variations in total NF-κB and due to extrinsic variations in IKK. Comparison of the coefficient of variation (CV) for peak and late-phase nuclear NF-κB levels due to extrinsic variability in total NF-κB (A,C) and IKK (B,D) for the single feedback and dual feedback network.

latter reactions are initiated at times dictated by their respective rates, but the numbers of molecules are only updated after the time delay since the reaction initiation. In contrast to recent stochastic models of NF-κB signaling which assume that the main source of stochasticity in gene expression is due to infrequent binding and dissociation of NF-κB from regulatory sites (Lipniacki *et al*, 2006; Ashall *et al*, 2009), our stochastic model utilizes much higher binding and dissociation rates which is consistent with *in vivo* analysis of NF-κB activation (Bosisio *et al*, 2006). In our stochastic model, discrete protein synthesis events are the main source of stochasticity.

We ran stochastic simulations of both a single and dual feedback system and and estimated the ensemble average $\langle X \rangle$ of the number of NF-κB molecules X and the magnitude of fluctuations as characterized by the standard deviation $\Delta X = [\langle X - \langle X \rangle \rangle^2]^{1/2}$ and the coefficient of variation $CV = \Delta X / \langle X \rangle$. To determine how the variability in the response varies with the magnitude of the input and the size of the system, we determined the CV in peak nuclear NF-κB levels and the CV in late-phase nuclear NF-κB levels for several values of IKK (Figure 3.14*A,C*) and for systems with up to 100,000 NF-κB molecules (Figure 3.14*B,D*). In Figure 3.14, we also plot CV values for extrinsic variations ($\pm$20%) in total NF-κB at several values of IKK (Figure 3.14*A,C*) and CV values for extrinsic variations in IKK ($\pm$20%) for several different system sizes (Figure 3.14*B,D*). We find that, even with this relatively low level ($\pm$20%) of extrinsic variability in IKK and NF-κB protein levels (Dower and Qwarnstrom, 2003), variability in the response of the network is dominated by extrinsic noise for large systems ($> 10,000$ NF-κB molecules).

The CV in late-phase nuclear NF-κB levels is similar for extrinsic and

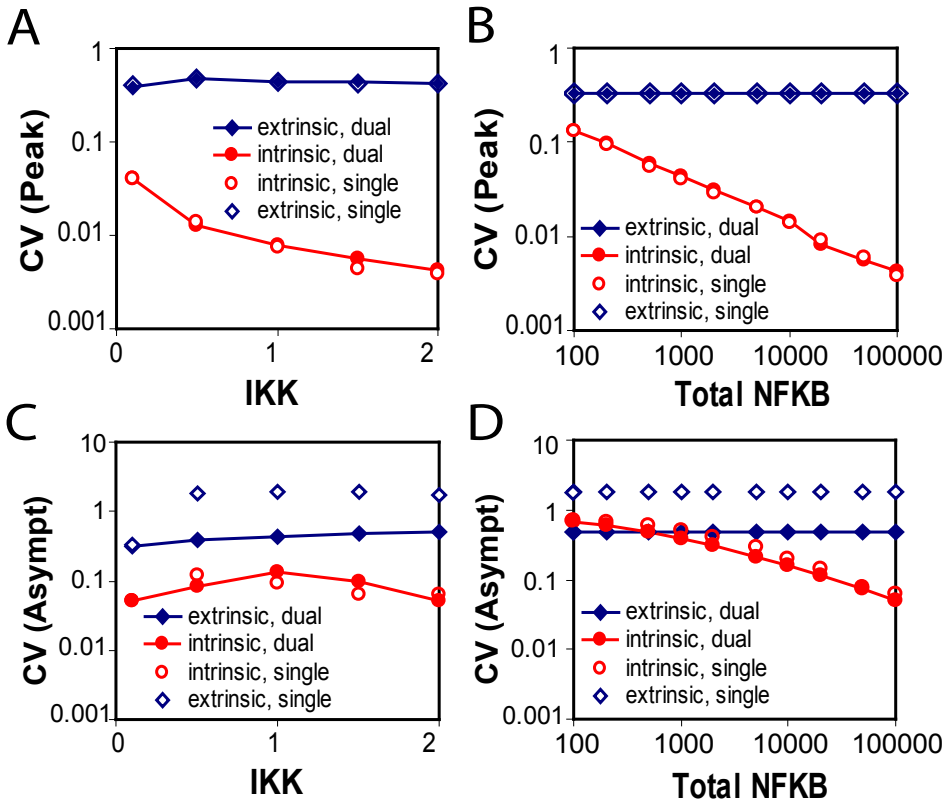

Figure 3.14: CV for peak and late-phase nuclear NF-κB levels due to extrinsic and intrinsic fluctuations. The CV due to intrinsic fluctuations was determined from at least 50 runs of the stochastic simulations at each value of IKK (A,C) and total NF-κB (B,D). The CV due to extrinsic fluctuations in total NF-κB and IKK levels was determined by varying the total NF-κB level by $\pm 20\%$ for each value of IKK (A,C) and by varying IKK by $\pm 20\%$ for value of total NF-κB (B,D). Work done with colleague Lev Tsimring.

intrinsic noise when the size of the system is reduced to 1000 NF-κB molecules. Next, we investigated the behavior of the NF-κB signaling module in this regime where intrinsic noise levels become significant by analyzing stochastic simulations produced with a system with total NF-κB levels set to 1000 molecules. We ran stochastic simulations of all three systems studied deterministically above (Figure 3.9): no-feedback, single negative feedback, and dual negative feedback (Figure 3.15). Note that ensemble-averaged runs agree with the deterministic simulations very well (Figure 3.17).

In the case of no feedback (Figure 3.15A) there is a strong robust response to the incoming persistent signal as characterized by the low values of the coefficient of variation. However, as we have seen above in Figure 3.9, the major flaw of this system is its slow response to the pulse-like signals. Next, we simulated the 9 biochemical reactions included in the IκBα-mediated single negative feedback loop (Figure 3.15B). In single runs the first peak in nuclear NF-κB levels appears to be very robust, as illustrated by Figure 3.15B *Top*. The CV is lowest (< 0.2) during the first peak in nuclear NF-κB indicating that this portion of the response is very robust.

Next, we performed stochastic simulations of the 18 biochemical reactions included in the dual delayed feedback model (with both IκBα- and IκBϵ-mediated feedback) (Figure 3.15C). In the dual feedback model, as in the single IκBα-mediated feedback model, there is a very robust first peak. However, unlike the single IκBα-mediated feedback model, in the dual feedback system the noise levels remain at a low level ($< .5$) following the first peak in nuclear NF-κB (Figure 3.15C *Bottom*). Thus, the dual feedback architecture allows for lower noise levels also in the later portion of the response.

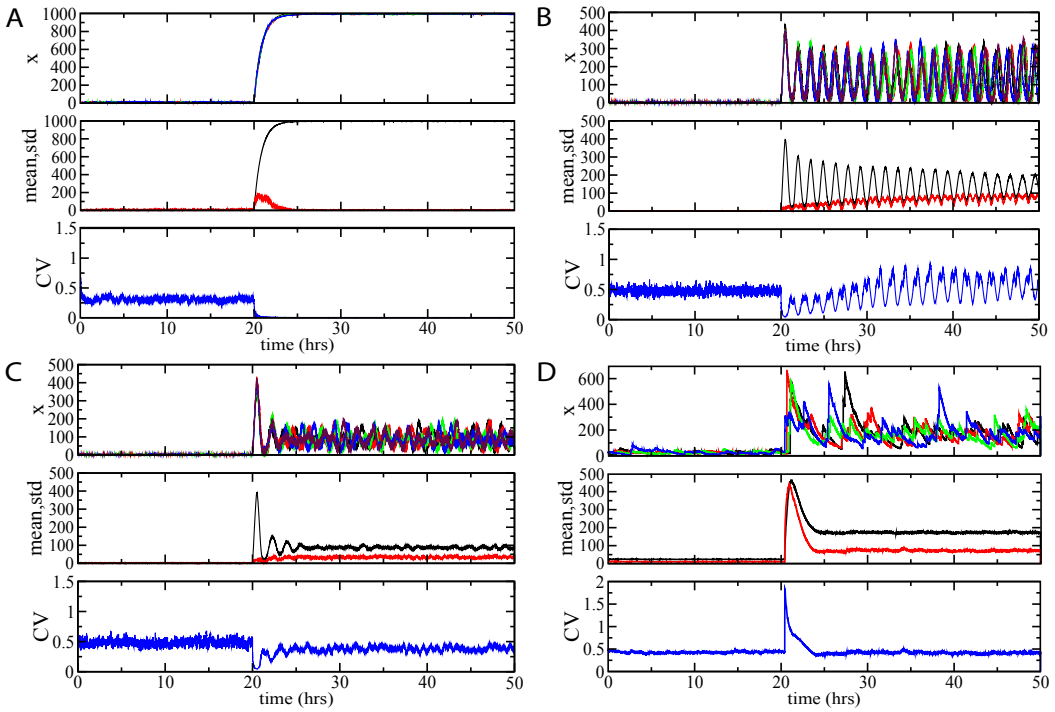

Figure 3.15: Stochastic simulation results for the NF-κB network with 1000 total NF-κB molecules. Stochastic simulation results for the NF-κB network with no feedback loops (A), only IκBα-mediated negative feedback (B), the NF-κB network with both IκBα- and IκBϵ-mediated negative feedback (C), and an alternative auto-repressive network (D). The top panel in each group shows four typical runs of stochastic simulations for each network, the middle panel shows the mean and standard deviation for 200 runs of each network, and the bottom panel shows the corresponding coefficient of variation. The input signal, K(t), is switched from $K = 0$ to $K = K_{max}$ at $t = 20$ hrs. In A-C, the magnitude of external signal $K_{max} = 2$, in D, $K_{max} = 50$. Work done by colleague Lev Tsimring.

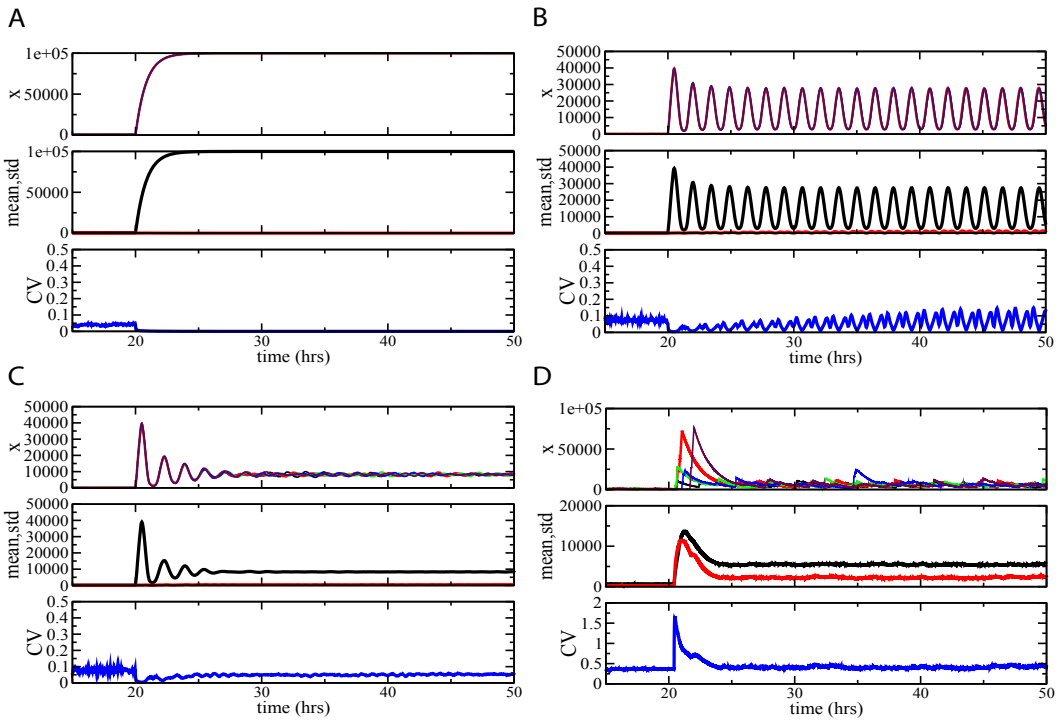

Figure 3.16: Stochastic simulation results for the NF-κB network with 100,000 total NF-κB molecules. Stochastic simulation results for the NF-κB network with no feedback loops (A), only IκBα-mediated negative feedback (B), the NF-κB network with both IκBα- and IκBϵ-mediated negative feedback (C), and an alternative auto-repressive network (D). The top panel in each group shows four typical runs of stochastic simulations for each network, the middle panel shows the mean and standard deviation for 200 runs of each network, and the bottom panel shows the corresponding coefficient of variation. The input signal, K(t), is switched from $K = 0$ to $K = K_{max}$ at $t = 20$ hrs. In A-C, the magnitude of external signal $K_{max} = 2$, in D, $K_{max} = 50$. Work done by colleague Lev Tsimring.

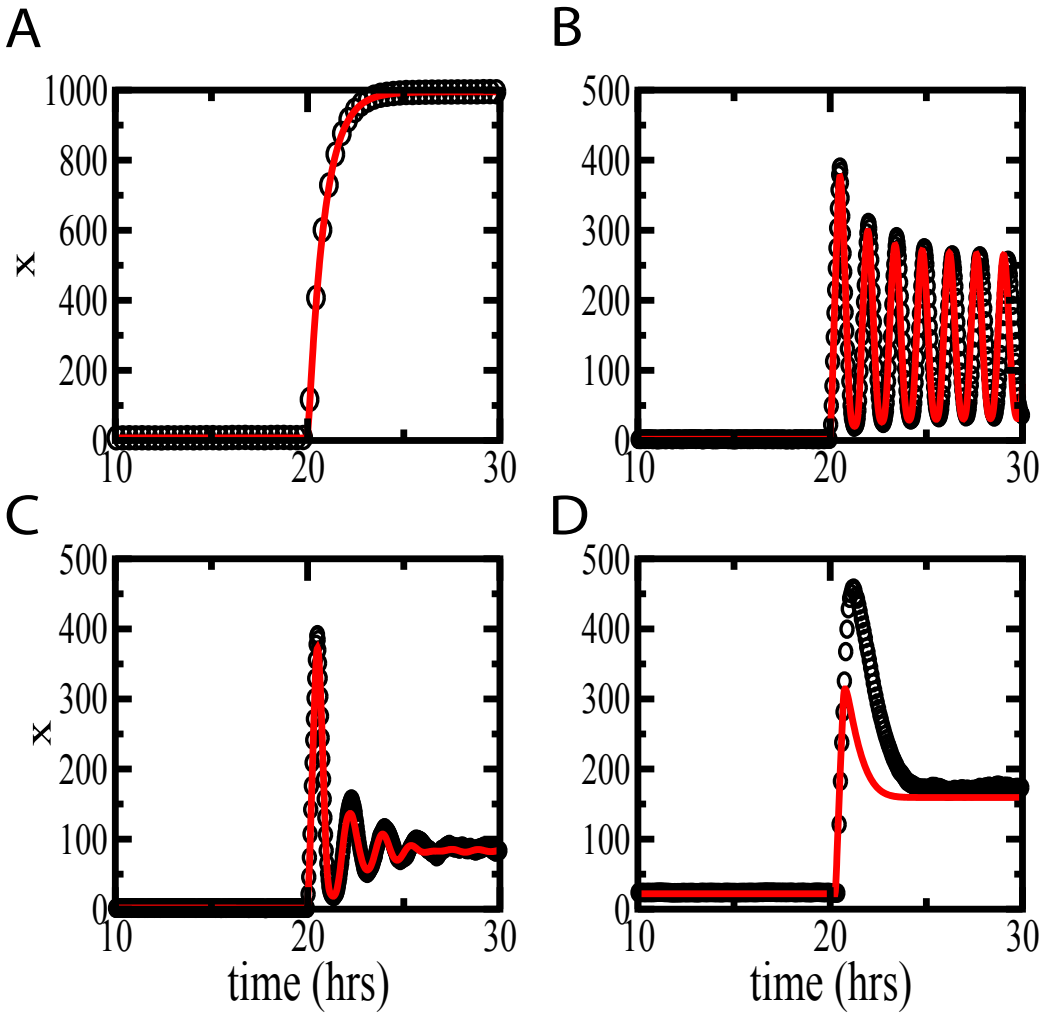

Figure 3.17: Comparison of stochastic and deterministic simulations. No-feedback model (A), single negative feedback model (B), dual feedback system (C), and auto-repressor system (D). Lines - deterministic simulations, symbols - stochastic simulations averaged over 200 runs. Work done by colleague Lev Tsimring.

What is the underlying reason for the robustness of the initial response from this circuit? To answer this question we need to realize that the main source of intrinsic noise in the system is presumably in the transcription and translation of IκB isoforms, since they are transcribed from single genes. In contrast, the contribution of degradation and transport processes to fluctuations is relatively small, because the copy numbers of the corresponding protein molecules are large. In the NF-κB network, the peak in nuclear NF-κB levels that occurs following stimulation is produced via the degradation of IκB proteins that bind and sequester NF-κB in the cytoplasm. Thus, we hypothesize that robustness of the initial response of the NF-κB circuit is explained by the fact that it uses the sequestering mechanism and does not rely on the protein production.

To test this hypothesis, we simulated the behavior of an alternative network that relies on transcription of auto-repressor, rather than the degradation of inhibitor proteins, for signaling (Figs. 3.15D, 3.18). This system can be modeled with two variables: x, the number of repressor molecules, and d, the binary state of the promoter ($d = 0$ corresponds to the unbound promoter and $d = 1$ corresponds to bound promoter), and with four reactions (binding and unbinding of the repressor to the promoter, degradation of the repressor, and delayed synthesis of the repressor with rate $K(t)(1 - d)$ where $K(t)$ is the external signal (Tables 3.4, 3.5). The input signal activates the production of the auto-repressor which after a certain time delay binds to the promoter and terminates further synthesis. Deterministically, this circuit also provides a desired response to a persistent stimulation with a large well-defined first peak.

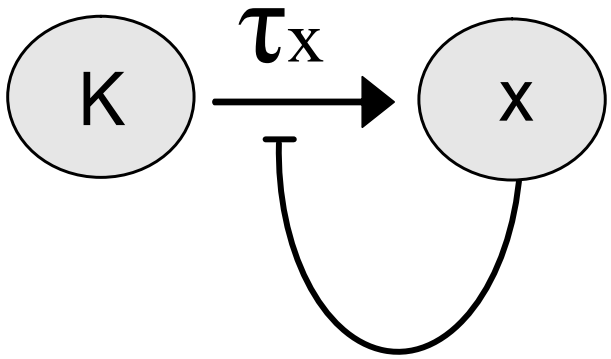

Figure 3.18: Alternative auto-repressive network. The external signal K activates the synthesis of the auto-repressor x which then binds to the promoter and inhibits further synthesis.

However, stochastic simulations reveal significant differences in the noise performance of this design as compared with the NF-κB circuit (note that the agreement between deterministic and stochastic simulations is less accurate in this case because of the strong promoter fluctuations, see Figure 3.17D). Activation of the auto-repressor network is much less robust than the activation of the NF-κB network (cf. Figure 3.15D and Figs. 3.15B, C). In fact, in the auto-repressor network, the coefficient of variation is highest (>1) during the initial peak (Figure 3.15D *Bottom*). These results confirm our conjecture that the sequestering mechanism incorporated in the design of the NF-κB network gives rise to a much more robust activation of NF-κB than alternative networks that rely on transcription for activation and signaling. This finding is in accord with recent work (Doncic et al., 2006) where the sequestering of Cdc20 protein was also implicated in the noise resistance of the spindle assembly checkpoint.

As mentioned previously, recent computational work has suggested that persistent oscillations are present in wild-type cells with both IκBα- and IκBϵ-mediated feedback but desynchronization due to stochastic variation produces damped oscillations at the population level (Ashall et al., 2009). Our computational and experimental results demonstrate that, although stochastic oscillations are still present in individual cells with both IκBα- and IκBϵ-mediated feedback (Figure 3.15*C*), the oscillatory propensity is greatly reduced by the second feedback loop in the wild-type NF-κB signaling module. Further, stochastic simulations of the dual-feedback network reveal highly synchronized damped oscillations (Figure 3.16C) with cellular variations in frequency due to intrinsic noise becoming significant only when the system size is drastically

reduced (Figure 3.15C).

3.7 Discussion

In this work we have developed a model of the NF-κB signaling pathway that uses a small number of reactions (some of them compound) thus making it amenable to mathematical analysis. Previously, a minimal model of NF-κB signaling was developed in which a massive overshoot in IκBα resulted in an effective slowing of signaling dynamics (Krishna et al., 2006), and produced spiky oscillations that are not seen in physiological conditions. Our model, which utilizes an explicit time delay, recapitulates experimentally observed signaling behavior. We suggest that models with an explicit time delay are useful for investigating the mechanistic basis of the dynamic behavior of signaling pathways.

Using this model, we explored the potential role of NF-κB oscillations which are observed in a variant of the NF-κB signaling module with the secondary negative feedback loop involving IκBϵ, disabled. In particular, we addressed the question of whether the frequency of these oscillations contains information, as in neurons which sometimes encode information in the frequency of action potentials (Bean, 2007) and in the activation of the transcription factor NF-AT which is responsive to the frequency of Ca^{2+} oscillations (Dolmetsch et al., 1998). By analyzing the oscillatory response of a system regulated solely by the IκBα-mediated negative feedback loop, we found that both the frequency and the decay rate of the oscillations produced by this system are highly dependent on the internal parameters of the circuit, but are not sensitive to changes in the input signal levels. This result suggests that the

oscillatory frequency does not encode information about the stimulus. Hence, stimulus-specific gene expression is unlikely determined by stimulus-specific frequencies of NF-κB oscillations. If there is a temporal code for stimulus-specific gene expression it is unlikely to involve frequency modulation, but may involve amplitude modulation over time.

When a second feedback regulator, IκBϵ, is added to the model, the oscillations caused by turning on a persistent IKK stimulus are significantly dampened, in agreement with our earlier findings (Kearns et al., 2006). By performing an optimization procedure, we determined that the specific experimentally observed parameter values for the synthesis delay and peak protein abundance of both IκB isoforms correspond to maximal efficiency of damping. These findings strongly suggest that the second feedback (IκBϵ) has specifically evolved to produce maximal damping of the oscillatory behavior of the first feedback (IκBα).

Thus, from the evolutionary perspective we have a peculiar situation in which a signaling module apparently first developed a negative feedback loop that made it prone to oscillations, and then added a secondary loop which mitigated these oscillations. This brings the question, if oscillatory responses are not beneficial to the cell, why has the primary negative feedback appeared in the system in the first place? By comparing transient response of several variants of signaling modules (0-, 1- and 2-feedback loop designs) in the presence of stochastic fluctuations we showed that the primary negative feedback loop involving the release of sequestered NF-κB proteins created a strong, rapid, and robust response to short pulses of IKK signal. However, for longer signals a single-feedback-loop system exhibits a suboptimal "temporal dose response

behavior" that leads to a quantized response to signals of different durations. In contrast, the dual feedback network generates response durations that are proportional to the stimulus input durations. Fine-tuning of the response duration that is reflective of the precise stimulus duration may be critical for gene expression programs that are activated by the second phase of NF-κB activity. In that sense, the regulatory mechanisms in the NF-κB system may be similar to those proposed in the p53 regulatory system that allow for discrete pulses of activities that regulate DNA repair and apoptosis (Ma et al., 2005).

3.8 Materials and Methods

3.8.1 Cell culture experiments

Immortalized murine embryonic fibroblasts (Hoffmann et al., 2002) were chronically stimulated with 10ng/mL TNF (Roche) and IκBα and IκBϵ mRNA and protein levels were monitored by RNase Protection Assay (RPA) and Western Blot, respectively, as previously described (Kearns et al., 2006). RPA results for each time course were quantitated using ImageQuant software (GE Healthcare) and used to determine the time of half-maximal inducibility between basal and peak mRNA levels for IκBα and IκBϵ (Figure 3.7A, B). Western Blot results were also quantitated with ImageQuant software and used to determine the time point of peak expression. The basal abundances of IκBα and IκBϵ protein were determined via comparison to a standard curve of recombinant IκB protein (JD Kearns, S Basak, C Lynch, A Hoffmann *in preparation*). The peak abundances of IκBα and IκBϵ were determined via multiplication of the basal value by the fold inducibility at the peak time point (Figure 3.7C, D). Experimental levels of nuclear NF-κB in cells with only the

IκBα-mediated negative feedback loop intact and in wild-type cells containing both IκBα- and IκBϵ-mediated negative feedback were determined by EMSAs in Hoffmann et al., 2002.

3.8.2 Derivation of the deterministic model

Using mass action kinetics, the full set of reactions for the dual feedback loop NF-κB system (Table 3.2, A and B) can be expressed by the following ODEs:

$$\dot{x} = -f_0 d_{0y} x + f_1 d_{1y} - k_y yx + k_{-y}[xy] + Kr_y[xy] - f_0 d_{0z} x + f_1 d_{1z} - k_z zx + k_{-z}[xz] + Kr_z[xz] \tag{3.10}$$

$$\dot{[xy]} = k_y yx - k_{-y}[xy] - Kr_y[xy] \tag{3.11}$$

$$\dot{y} = a_y d_{0y}(t-\tau_y) + b_y d_{1y}(t-\tau_y) - k_y yx + k_{-y}[xy] - g_y y - Kr_y y \tag{3.12}$$

$$\dot{d_{0y}} = -f_0 d_{0y} x + f_1 d_{1y} \tag{3.13}$$

$$\dot{d_{1y}} = f_0 d_{0y} x - f_1 d_{1y} \tag{3.14}$$

$$\dot{[xz]} = k_z zx - k_{-z}[xz] - Kr_z[xz] \tag{3.15}$$

$$\dot{z} = a_z d_{0z}(t-\tau_z) + b_z d_{1z}(t-\tau_z) - k_z zx + k_{-z}[xz] - g_z z - Kr_z z \tag{3.16}$$

$$\dot{d_{0z}} = -f_0 d_{0z} x + f_1 d_{1z} \tag{3.17}$$

$$\dot{d_{1z}} = f_0 d_{0z} x - f_1 d_{1z} \tag{3.18}$$

The total number of κB binding sites on each promoter is conserved:

$$d_{0y} + d_{1y} = d_y \tag{3.19}$$

$$d_{0z} + d_{1z} = d_z \tag{3.20}$$

We assume that the total amount of NF-κB in the cell X is conserved

$$X = x + d_{1y} + d_{1z} + [xy] + [xz] = const. \tag{3.21}$$

Since the number of binding sites available for NF-κB protein is small, we can neglect the amount of NF-κB bound to the IκBα and IκBϵ promoters, so

$$X = x + [xy] + [xz] \tag{3.22}$$

Solving Eq. 3.22 for x yields:

$$x = X - [xy] + [xz] \tag{3.23}$$

DNA binding reactions are usually fast, so we can assume that they are at quasi-equilibrium at all times,

$$f_1 d_{1y} = f_0 d_{0y} x \tag{3.24}$$

$$f_1 d_{1z} = f_0 d_{0z} x \tag{3.25}$$

Using Eqs. 3.19 and 3.20, substituting into Eqs. 3.24 and 3.25, and solving for d_{0y}, d_{1y}, d_{0z}, d_{1z} yields:

$$d_{0y} = \frac{f_1 d_y}{f_1 + f_0 x} \tag{3.26}$$

$$d_{1y} = \frac{f_0 x d_y}{f_1 + f_0 x} \tag{3.27}$$

$$d_{0z} = \frac{f_1 d_z}{f_1 + f_0 x} \tag{3.28}$$

$$d_{1z} = \frac{f_0 x d_z}{f_1 + f_0 x} \tag{3.29}$$

We also assume quasi-equilibrium for IκB-NF-κB binding reactions,

$$k_y y x = k_{-y}[xy] + Kr_y[xy] \tag{3.30}$$

$$k_z zx = k_{-z}[xz] + Kr_z[xz] \tag{3.31}$$

Substituting $[xy]$ and $[xz]$ from Eqs. 3.30 and 3.31 into Eq. 3.23 yields:

$$x = X - [k_y yx/(k_{-y} + Kr_y)] - [k_z zx/(k_{-z} + Kr_z)] \tag{3.32}$$

Now we can solve Eq. 3.32 for x

$$x = \frac{X}{1 + k_y y/(k_{-y} + Kr_y) + k_z z/(k_{-z} + Kr_z)} \tag{3.33}$$

and substitute it in Eqs. 3.12 and 3.16. These equations contain both fast and slow terms. However, it is easy to see that rate equations for variables $Y = y + [xy]$ and $Z = z + [xz]$ contain only slow terms:

$$\dot{Y} = a_y d_{0y}(t - \tau_y) + b_y d_{1y}(t - \tau_y) - g_y y - Kr_y Y \tag{3.34}$$

$$\dot{Z} = a_z d_{0z}(t - \tau_z) + b_z d_{1z}(t - \tau_z) - g_z z - Kr_z Z \tag{3.35}$$

Y and Z can in turn be expressed via y and z by:

$$Y = y[1 + c_y X/(1 + c_y y + c_z z)] \tag{3.36}$$

$$Z = z[1 + c_z X/(1 + c_y y + c_z z)] \tag{3.37}$$

where $c_y = k_y/(k_{-y} + Kr_y)$ and $c_z = k_z/(k_{-z} + Kr_z)$. Eqs. 3.34–3.35 combined with definitions Eqs. 3.26–3.29, 3.33, 3.36, and 3.37 represent a closed system of two delay-differential equations (Eqs. 3.8 and 3.9) for the dual-feedback NF-κB module. Setting $Z = z = 0$ in these equations leaves us with a single delay-differential equation for the single feedback loop system Eq. 3.1.

3.8.3 Details of the linear stability analysis

The linearized equation for the single delayed negative feedback system has the form

$$\dot{\xi} = B\xi_\tau - Kr_y\xi \tag{3.38}$$

where $\xi = Y - Y_s$, Y_s is the stationary level of Y, subscript τ again indicates the delayed value of ξ taken at time $t-\tau$, and $B = dG(Y_s)/dY$ is the Jacobian. The latter has the explicit form

$$B = \frac{2d_y b_y c_y^2 F\left[c_y(X - Y_s) - 1 + S\right]}{\left[2c_y F + c_y(X - Y_s) - 1 + S\right]^2 S} \tag{3.39}$$

where $S = \left[(c_y(X - Y_s) - 1)^2 + 4c_y X\right]^{1/2}$. This Jacobian depends on the stationary level of the IκBα expression Y_s. Unfortunately, Eq. 3.4 does not permit finding Y_s in explicit form. However, this calculation can be significantly simplified if the total number of NF-κB proteins is large, so $c_y X \gg 1$, then y can be neglected as compared with total Y. Then $x = X - Y$, and $d_{1y} = d_y(X - Y)/(F + X - Y)$, and the equation for Y simplifies:

$$\dot{Y} = \frac{b_y d_y (X - Y_\tau)}{F + X - Y_\tau} - Kr_y Y \tag{3.40}$$

Now the stationary level of Y can be found explicitly

$$Y_s = \frac{b_y d_y + Kr_y(F + X) - \sqrt{(b_y d_y + Kr_y(F + X))^2 - 4Kr_y b_y d_y X}}{2Kr_y} \tag{3.41}$$

Under the same conditions, the expression for the Jacobian B can also be

simplified,

$$B = \frac{b_y d_y F}{(F + X - Y_s)^2} \tag{3.42}$$

3.8.4 Details of the BLASTP search for IκBα and IκBϵ homologs

We performed two BLASTP searches (using default parameters) to search for IκBα and IκBϵ homologs. For the first search, the mouse IκBα protein sequence (gi28386026) was used as the query. The mouse IκBϵ protein sequence (gi2739158) was used as the query for the second search. We used an E-value of 1e-25 as a cutoff for both searches. Homologs for IκBα were found in the organisms listed in Table 3.6, and homologs for IκBϵ were found in the organisms listed in Table 3.7.

Note that we did not find unique homologs for both IκBα and IκBϵ in all vertebrates. Only a single IκB homolog was found in the following vertebrates: Meriones unguiculatus, Macaca fascicularis, Gorilla gorilla, Pan paniscus, Gyps fulvus, Pongo pygmaeus, Oncorhynchus mykiss, Siniperca chuatsi, Ovis aries, Paralichthys olivaceus, Saguinus labiatus, Ateles geoffroyi, Lagothrix lagotricha, and Lemur catta. We expect that this is due to the fact that complete genomes are not currently available for these organisms. Table 3.8 lists the genome status (as of 1/6/09) of all organisms for which IκBα or IκBϵ homologs were found (http://www.ncbi.nlm.nih.gov/genomes/leuks.cgi).

3.9 Acknowledgements

Chapter 3 contains material to be submitted as Longo D, Kearns JD, Hoffmann A, Hasty J, Tsimring LS. Dual delayed feedback provides sensi-

tivity and robustness to the NF-κB signaling module. *Mol Syst Biol.* The dissertation author was the primary investigator and author of this paper.

Table 3.1: NF-κB model variables

A

Variable	**Description**
x	nuclear NF-κB (nM)
y	free IκBα (nM)
$[xy]$	NF-κB-bound IκBα (nM)
K	IκB kinase (IKK)
d_{0y}	unbound IκBα promoter*
d_{1y}	NF-κB-bound IκBα promoter*

B

Variable	**Description**
z	free IκBϵ (nM)
$[xz]$	NF-κB-bound IκBϵ (nM)
d_{0z}	unbound IκBϵ promoter*
d_{1z}	NF-κB-bound IκBϵ promoter*

*these are average numbers of corresponding promoters

Table 3.2: NF-κB model reactions

A

Reaction	**Rate**	**Description**
$d_{0y} + x \leftrightarrow d_{1y}$	f_0, f_1	NF-κB binds (and unbinds) IκBα promoter
$d_{0y} \rightarrow d_{0y} + y$	a_y	constitutive synthesis of IκBα (delayed reaction)
$d_{1y} \rightarrow d_{1y} + y$	b_y	induced synthesis of IκBα (delayed reaction)
$x + y \leftrightarrow [xy]$	k_y, k_{-y}	IκBα association (and dissociation) with NF-κB
$y \rightarrow \phi$	g_y	constitutive degradation of IκBα
$K + y \rightarrow K$	r_y	IKK-mediated degradation of IκBα
$K + [xy] \rightarrow K + x$	r_y	IKK-mediated degradation of NF-κB-bound IκBα

B

Reaction	**Rate**	**Description**
$d_{0z} + x \leftrightarrow d_{1z}$	f_0, f_1	NF-κB binds (and unbinds) IκBϵ promoter
$d_{0z} \rightarrow d_{0z} + z$	a_z	constitutive synthesis of IκBϵ (delayed reaction)
$d_{1z} \rightarrow d_{1z} + z$	b_z	induced synthesis of IκBϵ (delayed reaction)
$x + z \leftrightarrow [xz]$	k_z, k_{-z}	IκBϵ association (and dissociation) with NF-κB
$z \rightarrow \phi$	g_z	constitutive degradation of IκBϵ
$K + z \rightarrow K$	r_z	IKK-mediated degradation of IκBϵ
$K + [xz] \rightarrow K + x$	r_z	IKK-mediated degradation of NF-κB-bound IκBϵ

Table 3.3: NF-κB model parameter values

	Parameter Description	**Model Value****	**Ref. Value**
a_y	IκBα constitutive synthesis*	0.00185 nM/min	0.0185 nM/min[1]
b_y	IκBα inducible synthesis*	5.0 nM/min	138.6 nM/min[1]
d_y	IκBα promoter: number κB sites	1.0	
f_0	NF-κB binding IκB promoter	10.0 /(nMmin)	
f_1	NF-κB unbinding IκB promoter	200.0/min	
τ_y	Delay in IκBα synthesis	25.0 min	25.8 min[2]
k_y	IκBα binding with NF-κB	0.1 /(nMmin)	0.03 /(nMmin)[1]
k_{-y}	IκBα dissociates from NF-κB	0.0006/min	0.00006/min[1]
X	Total NF-κB	100 nM	100 nM[3]
g_y	Constitutive IκBα degradation	0.012/min	0.12/min[1]
r_y	Degradation of IκBα by IKK	0.01/min	0.018/min[1]
a_z	IκBϵ constitutive synthesis*	0.00046 nM/min	0.0046 nM/min[1]
b_z	IκBϵ inducible synthesis*	5.0 nM/min	18.0 nM/min[1]
d_z	IκBϵ promoter: number κB sites	1.0	
τ_z	Delay in IκBϵ synthesis	72.0 min	59.4 min[2]
k_z	IκBϵ binding with NF-κB	0.1 /(nMmin)	0.03 /(nMmin)[1]
k_{-z}	IκBϵ dissociates from NF-κB	0.0006/min	0.00006/min[1]
g_z	Constitutive IκBϵ degradation	0.018/min	0.18/min[1]
r_z	Degradation of IκBϵ by IKK	0.01/min	0.018/min[1]

*per 1 κB site

**1 nM = 1000 molecules for a cell volume that is on the order of 1 pico liter

[1] Kearns et al., 2006

[2] this work

[3] Hoffmann et al., 2002

Table 3.4: Auto-repressor network reactions

Reaction	**Rate**	**Description**
$d_0 + x \leftrightarrow d_1$	k_y, k_{-y}	binding and unbinding of repressor to the promoter
$x \rightarrow \phi$	g_y	degradation of the repressor
$d_0 \rightarrow d_0 + x$	$a_y(1 + K)$	synthesis of the repressor (delayed reaction)

Table 3.5: Auto-repressor network parameter values

	Parameter Description	**Parameter Value**
a_y	repressor synthesis rate	1.0 nM/min
g_y	repressor degradation rate	.012/min
k_y	binding of repressor to promoter	.1 nM/min
k_{-y}	unbinding of repressor from promoter	.06/min
τ_z	delay in synthesis of repressor	25.0 min

Table 3.6: Organisms with homologs for IκBα

Organism	**NCBI gi number**	**E-value**
Mus musculus	28386026	0
Rattus norvegicus	160333919	0
Meriones unguiculatus	108860577	2.00E-176
Sus scrofa	52346212	5.00E-169
Canis lupus familiaris	73963074	6.00E-169
Bos taurus	114052817	1.00E-168
Macaca mulatta	109083336	3.00E-167
Macaca fascicularis	90080313	3.00E-167
Homo sapiens	10092619	6.00E-167
Monodelphis domestica	126283568	1.00E-147
Ornithorhynchus anatinus	149548454	5.00E-138
Gorilla gorilla	120974064	1.00E-126
Equus caballus	194207294	4.00E-126
Pan paniscus	121483818	1.00E-125
Gyps fulvus	159895428	2.00E-120
Pongo pygmaeus	124054120	3.00E-118
Pan troglodytes	124111100	2.00E-117
Gallus gallus	126723285	1.00E-116
Xenopus tropicalis	52345606	2.00E-95
Xenopus laevis	148230967	3.00E-94
Oncorhynchus mykiss	185134623	2.00E-80
Salmo salar	209737318	6.00E-80
Siniperca chuatsi	133872756	7.00E-73
Danio rerio	37725732	2.00E-72
Ovis aries	165940914	1.00E-69
Paralichthys olivaceus	133779815	3.00E-65
Macaca nemestrina	124013515	1.00E-63
Tetraodon nigroviridis	47209080	2.00E-63
Saguinus labiatus	121221930	5.00E-61
Ateles geoffroyi	122053822	1.00E-57
Lemur catta	122938174	8.00E-45
Apis mellifera	110756132	9.00E-35
Carcinoscorpius rotundicauda	71738527	9.00E-33
Biomphalaria glabrata	119393872	9.00E-32
Crassostrea gigas	80971720	3.00E-30
Nasonia vitripennis	156543541	5.00E-30
Lutzomyia longipalpis	149728129	1.00E-29
Pinctada fucata	194718237	2.00E-29
Drosophila yakuba	195475366	4.00E-29
Aedes aegypti	157108525	5.00E-29
Pediculus humanus corporis	212512255	6.00E-29

Table 3.6 cont.

Organism	**NCBI gi number**	**E-value**
Drosophila willistoni	195433326	7.00E-29
Euprymna scolopes	63034007	7.00E-29
Drosophila erecta	194857830	1.00E-28
Drosophila grimshawi	195034537	1.00E-28
Drosophila melanogaster	17136840	1.00E-28
Drosophila virilis	195386110	1.00E-28
Drosophila mojavensis	195114618	3.00E-28
Drosophila ananassae	194759838	4.00E-28
Drosophila persimilis	195160098	4.00E-28
Drosophila pseudoobscura pseudoobscura	198475712	4.00E-28
Nematostella vectensis	156079906	9.00E-28
Strongylocentrotus purpuratus	72004276	2.00E-27
Ciona intestinalis	118343834	2.00E-27
Tribolium castaneum	91093127	8.00E-27
Anopheles gambiae str. PEST	118789617	3.00E-26
Drosophila simulans	195579553	9.00E-26

Table 3.7: Organisms with homologs for IκBϵ

Organism	**NCBI gi number**	**E-value**
Mus musculus	2739158	0
Rattus norvegicus	40018590	0
Sus scrofa	194039395	2.00E-162
Bos taurus	195539539	4.00E-161
Pan troglodytes	114607603	7.00E-154
Homo sapiens	20530139	1.00E-153
Macaca mulatta	109071331	3.00E-150
Monodelphis domestica	126310114	3.00E-129
Canis familiaris	73973023	1.00E-89
Xenopus tropicalis	187608250	4.00E-81
Xenopus laevis	147907302	5.00E-74
Danio rerio	121583661	6.00E-62
Salmo salar	213514346	3.00E-61
Tetraodon nigroviridis	47224342	4.00E-53
Gallus gallus	118088055	2.00E-38
Ornithorhynchus anatinus	149542664	8.00E-36
Nematostella vectensis	156079906*	1.00E-33
Carcinoscorpius rotundicauda	71738527*	3.00E-33
Strongylocentrotus purpuratus	72004276*	5.00E-33
Biomphalaria glabrata	119393872*	6.00E-32
Euprymna scolopes	63034007*	1.00E-31
Pinctada fucata	194718237*	1.00E-31
Siniperca chuatsi	133872756*	1.00E-30
Oncorhynchus mykiss	185134623*	1.00E-30
Aedes aegypti	157108525*	2.00E-30
Equus caballus	194205729	1.00E-29
Macaca fascicularis	90080313*	4.00E-29
Crassostrea gigas	80971720*	8.00E-29
Gyps fulvus	159895428*	2.00E-28
Ciona intestinalis	118343834*	4.00E-28
Apis mellifera	110756132*	1.00E-27
Drosophila melanogaster	17136840*	4.00E-27
Drosophila erecta	194857830*	4.00E-27
Meriones unguiculatus	108860577*	5.00E-27
Drosophila yakuba	195475366*	7.00E-27
Paralichthys olivaceus	133779815*	9.00E-27
Drosophila ananassae	194759838*	1.00E-26
Nasonia vitripennis	156543541*	8.00E-26

Table 3.7 cont.

Organism	**NCBI gi number**	**E-value**
Drosophila persimilis	195160098*	1.00E-25
Drosophila pseudoobscura pseudoobscura	198475712*	1.00E-25
Drosophila mojavensis	195114618*	1.00E-25
Gorilla gorilla	120974064*	2.00E-25
Pan paniscus	121483818*	5.00E-25

*These sequences are the same sequences that were found with the IκBα search. Therefore, these organisms do not have unique homologs for IκBα and IκBϵ.

Table 3.8: Genome status of organisms in Tables 3.6 and 3.7

Organism	**Common name**	**Genome status**
Aedes aegypti	mosquito	Assembly
Anopheles gambiae str. PEST	mosquito	Assembly
Apis mellifera	honey bee	Assembly
Ateles geoffroyi	spider monkey	Not found
Biomphalaria glabrata	snail	In Progress
Bos taurus	cow	Assembly
Canis lupus familiaris	dog	Assembly
Carcinoscorpius rotundicauda	horseshoe crab	Not found
Ciona intestinalis	sea squirt	Assembly
Crassostrea gigas	pacific oyster	Not found
Danio rerio	zebrafish	In Progress
Drosophila ananassae	fly	Assembly
Drosophila erecta	fly	Assembly
Drosophila grimshawi	fly	Assembly
Drosophila melanogaster	fruit fly	Complete
Drosophila mojavensis	fly	Assembly
Drosophila persimilis	fly	Assembly
D. pseudoobscura pseudoobscura	fly	Assembly
Drosophila simulans	fly	Assembly
Drosophila virilis	fly	Assembly
Drosophila willistoni	fly	Assembly
Drosophila yakuba	fly	Assembly
Equus caballus	horse	Assembly
Euprymna scolopes	squid	Not found
Gallus gallus	chicken	Assembly
Gorilla gorilla	gorilla	Assembly
Gyps fulvus	vulture	Not found
Homo sapiens	human	Complete
Lagothrix lagotricha	woolly monkey	Not found
Lemur catta	lemur	In Progress
Lutzomyia longipalpis	sandfly	Not found
Macaca fascicularis	macaque	In Progress
Macaca mulatta	monkey	Assembly
Macaca nemestrina	macaque	Not found
Meriones unguiculatus	gerbil	Not found
Monodelphis domestica	opossum	Assembly
Mus musculus	mouse	Complete
Nasonia vitripennis	wasp	Assembly
Nematostella vectensis	sea anemone	Assembly
Oncorhynchus mykiss	rainbow trout	Not found
Ornithorhynchus anatinus	platypus	In Progress
Ovis aries	sheep	Not found

Table 3.8 cont.

Organism	**Common name**	**Genome status**
Pan paniscus	bonobo	Not found
Pan troglodytes	chimp	Assembly
Paralichthys olivaceus	flounder	Not found
Pediculus humanus corporis	human body louse	Assembly
Pinctada fucata	oyster	Not found
Pongo pygmaeus	orangutan	Not found
Rattus norvegicus	rat	Assembly
Saguinus labiatus	tamarin monkey	Not found
Salmo salar	salmon	Not found
Siniperca chuatsi	mandarin fish	Not found
Strongylocentrotus purpuratus	sea urchin	Assembly
Sus scrofa	pig	In Progress
Tetraodon nigroviridis	pufferfish	Assembly
Tribolium castaneum	beetle	Assembly
Xenopus laevis	frog	Not found
Xenopus tropicalis	frog	In Progress

Chapter 4

Concluding remarks

Biological systems often consist of many components with numerous interactions between these components resulting in extremely complex network architectures. The recent emergence of the field of systems biology has provided novel theoretical and experimental tools for characterizing biological networks by identifying network components and interactions and determining the dynamic behavior and functions that arise from these interactions (Kitano 2002; Barabasi and Oltvai, 2004; Albert 2007).

In Chapter 2, we utilized a systems biology approach to analyze the dynamic response of a synthetic mammalian positive feedback network. In both our experiments and our stochastic simulations, we observed a switch-like activation of the network with variable delay times in individual cells. We found that a shorter mean delay time and a more coherent activation could be achieved by increasing the strength of the positive feedback. Similar signaling properties have been observed in naturally-occurring regulatory networks such as the network governing apoptosis in mammalian cells and in the cell

cycle regulatory network in *S. cerevisiae*. By utilizing our stochastic model, we demonstrated that the timing of activation is also quite sensitive to changes in the transcription rate of the activator. Thus, precise regulation of activator mRNA synthesis rates may serve as a mechanism for tuning the timing of activation in naturally-occurring biological networks. By constructing and characterizing a synthetic mammalian positive feedback network we have gained insight into the dynamic behavior of more complex naturally-occurring systems that contain positive feedback loops. Future work in the field of mammalian synthetic biology is expected to advance our understanding of the operating principles of complex biological systems and lead to further progress in areas such as drug discovery, tissue engineering, and biopharmaceutical manufacturing (Weber and Fussenegger, 2009).

In Chapter 3, we explored the dynamic activity of the transcription factor NF-κB that is produced by dual negative feedback loops. By utilizing our model of the NF-κB signaling pathway, we found that the frequency and decay rate of oscillations produced by the IκBα-mediated negative feedback loop are not sensitive to changes in the input signal levels suggesting that the oscillatory frequency does not encode information about the stimulus. We performed a parameter optimization procedure of the dual feedback network to determine the IκBϵ synthesis parameter values that result in maximum damping and found a good correspondence between the model prediction for optimal damping and experimental measurements of relevant parameter values indicating that the second IκBϵ-mediated feedback loop may have specifically evolved to minimize the oscillatory behavior of the first IκBα-mediated feedback loop. Further, we demonstrated that the dual feedback architecture

allows for a highly sensitive response to transient stimuli and a temporally graded response to longer inputs. Finally, we analyzed the variability in the response of the NF-κB module that arises due to intrinsic and extrinsic noise, and we found that the dual-feedback loop architecture allows for a more robust response than the single feedback loop system. By utilizing a systems biology approach that combines quantitative experimentation with theoretical modeling, we have gained novel insight into the function and origin of the NF-κB signaling system.

The development of systems-level approaches for quantitatively analyzing the dynamics of biological networks was spurred by the availability of the first draft sequences of the human genome in 2001 (International Human Genome Sequencing Consortium, 2001; Venter et al., 2001) and the completion of the Human Genome Project in 2003 (International Human Genome Sequencing Consortium, 2004). The introduction of novel technologies that enable genome-scale analyses has led to a transformation in biological research with studies examining the function of a single molecule in isolation being replaced by studies which examine the interactions of tens to thousands of molecules thus probing the behavior and function of whole networks.

While the original Human Genome Project cost billions of dollars and took several years to complete, it is estimated that advances in DNA sequencing technologies will allow for the sequencing of an entire human genome in several hours with a cost of $100 as soon as 2012 (http://www.BioNanomatrix.com; http://www.completegenomics.com). Currently, researchers involved in the 1000 Genomes Project are using novel sequencing technology to sequence the genomes of 1000 individuals which will allow single nucleotide polymorphisms

(SNPs) that occur at a frequency as low as 1% to be found (Kaiser 2008). Genome-wide association studies which examine statistical associations between SNPs and the occurrence of disease will lead to further discoveries about the biological pathways which underlie disease (Koenig 2009).

Rapid progress in DNA sequencing and DNA synthesis technologies (Gibson et al., 2008) has been accompanied by the development of novel experimental methods for characterizing signaling activity in individual cells. Recent studies have demonstrated that precise temporal stimuli with diverse patterns can be generated using microfluidic devices allowing for the observation of cellular responses to time-varying signals (Bennett et al., 2008; Hersen et al., 2008). Furthermore, the development of high content, high throughput assays has enabled quantitative measurements of multiple signaling species in single cells in response to various stimuli (Irish et al., 2006; Krutzik et al., 2008; Cheong et al., 2009). The production of profuse amounts of different types of data from diverse systems will necessitate advances in computational methods that allow for the integration of multiple data sets into models of biological networks. Through the iterative refinement of network models, we will deepen our understanding of cellular signaling in both healthy and diseased states thus leading to the development of more effective diagnostic and therapeutic approaches.

References

Albeck JG, Burke JM, Aldridge BB, Zhang M, Lauffenburger DA, Sorger PK (2008) Quantitative analysis of pathways controlling extrinsic apoptosis in single cells. *Mol Cell* **30**: 11–25.

Albert R (2007) Network inference, analysis, and modeling in systems biology. *Plant Cell* **19**: 3327–3338.

Arkin A, Ross J, McAdams HH (1998) Stochastic kinetic analysis of developmental pathway bifurcation in phage λ-infected *Escherichia coli* cells. *Genetics* **149**: 1633–1648.

Ashall L, Horton CA, Nelson DE, Paszek P, Harper CV, Sillitoe K, Ryan S, Spiller DG, Unitt JF, Broomhead DS, Kell DB, Rand DA, Se V, White MR (2009) Pulsatile stimulation determines timing and specificity of NF-kappaB-dependent transcription. *Science* **324**: 242–246.

Atkinson MR, Savageau MA, Myers JT, Ninfa AJ (2003) Development of genetic circuitry exhibiting toggle switch or oscillatory behavior in *Escherichia coli*. *Cell* **113**: 597-607.

Aurell E, Brown S, Johanson J, Sneppen K (2002) Stability puzzles in phage lambda. *Phys Rev E* **65**: 051914.

Austin DW, Allen MS, McCollum JM, Dar RD, Wilgus JR, Sayler GS, Samatova NF, Cox CD, Simpson ML (2006) Gene network shaping of inherent noise spectra. *Nature* **439**: 608-611.

Bar-Even A, Paulsson J, Maheshri N, Carmi M, O'Shea E, Pilpel Y, Barkai N (2006) Noise in protein expression scales with natural protein abundance. *Nat Genet* **38**: 636-643.

Barabsi AL, Oltvai ZN (2004) Network biology: understanding the cell's functional organization. *Nat Rev Genet* **5**: 101–113.

Barken D, Wang CJ, Kearns J, Cheong R, Hoffmann A, Levchenko A (2005) Comment on "Oscillations in NF-kappaB signaling control the dynamics of gene expression." *Science* **308**: 52.

Batchelor E, Mock CS, Bhan I, Loewer A, Lahav, G (2008) Recurrent initiation: a mechanism for triggering p53 pulses in response to DNA damage. *Mol Cell* **30**: 277–289.

Bean BP (2007) The action potential in mammalian central neurons. *Nat Rev Neurosci* **8**: 451–465.

Becskei A, Seraphin B, Serrano L (2001) Positive feedback in eukaryotic gene networks: cell differentiation by graded to binary response conversion. *EMBO J* **20**: 2528-2535.

Becskei A, Serrano L (2000) Engineering stability in gene networks by autoregulation. *Nature* **405**: 590-593.

Benner SA, Sismour AM (2005) Synthetic biology. *Nat Rev Genet* **6**: 533–543.

Bennett MR, Pang WL, Ostroff NA, Baumgartner BL, Nayak S, Tsimring LS, Hasty J (2008) Metabolic gene regulation in a dynamically changing environment. *Nature* **454**: 1119–1122.

BioNanomatrix Website. http://BioNanomatrix.com/. Accessed April 28, 2009.

Blake WJ, Kaern M, Cantor CR, Collins JJ (2003) Noise in eukaryotic gene expression. *Nature* **422**: 633-637.

Bosisio D, Marazzi I, Agresti A, Shimizu N, Bianchi ME, Natoli G (2006) A hyper-dynamic equilibrium between promoter-bound and nucleoplasmic dimers controls NF-kappaB-dependent gene activity. *EMBO J* **25**: 798–810.

Bratsun D, Volfson D, Tsimring LS, Hasty J (2005) Delay-induced stochastic oscillations in gene regulation. *Proc Natl Acad Sci USA* **102**: 14593–14598.

Cai L, Dalal CK, Elowitz MB (2008) Frequency-modulated nuclear localization bursts coordinate gene regulation. *Nature* **455**: 485–490.

Cheong R, Wang CJ, Levchenko A (2009) High content cell screening in a microfluidic device. *Mol Cell Proteomics* **8**: 433–442.

Cohen AA, Geva-Zatorsky N, Eden E, Frenkel-Morgenstern M, Issaeva I, Sigal A, Milo R, Cohen-Saidon C, Liron Y, Kam Z, Cohen L, Danon T, Perzov N, Alon U (2008) Dynamic Proteomics of Individual Cancer Cells in Response to a Drug. *Science* **332**: 1511–1516.

Colman-Lerner A, Gordon A, Serra E, Chin T, Resnekov O, Endy D, Pesce CG, Brent R (2005) Regulated cell-to-cell variation in a cellfate decision system. *Nature* **437**: 699-706.

Complete Genomics Website. http://completegenomics.com/. Accessed April

28, 2009.

Corish P, Tyler-Smith C (1999) Attenuation of green fluorescent protein half-life in mammalian cells. *Protein Eng* **12**: 1035–1040.

Dolmetsch RE, Xu K, Lewis RS (1998) Calcium oscillations increase the efficiency and specificity of gene expression. *Nature* **392**: 933–936.

Doncic A, Ben-Jacob E, Barkai N (2006) Noise resistance in the spindle assembly checkpoint. *Mol Syst Biol* **2**: 2006.0027.

Dower SK, Qwarnstrom EE (2003) Signalling networks, inflammation and innate immunity. *Biochem Soc Trans* **31**: 1462–1471.

Duggan DJ, Bittner M, Chen Y, Meltzer P, Trent JM (1999) Expression profiling using cDNA microarrays. *Nat Genet* **21**: 10–14.

Elowitz MB, Leibler S (2000) A synthetic oscillatory network of transcriptional regulators. *Nature* **403**: 335-338.

Elowitz MB, Levine AJ, Siggia ED, Swain PS (2002) Stochastic gene expression in a single cell. *Science* **297**: 1183–1186.

Endy D (2005) Foundations for engineering biology. *Nature* **438**: 449–453.

Ferber D (2004) Synthetic biology. Microbes made to order. *Science* **303**: 158–161.

Ferrell JE Jr, Machleder EM (1998) The biochemical basis of an all-or-none cell fate switch in Xenopus oocytes. *Science* **280**: 895–898.

Gardner TS, Cantor CR, Collins JJ (2000) Construction of a genetic toggle switch in Escherichia coli. *Nature* **403**: 339-342.

Gibson DG, Benders GA, Andrews-Pfannkoch C, Denisova EA, Baden-Tillson H, Zaveri J, Stockwell TB, Brownley A, Thomas DW, Algire MA, Merryman C, Young L, Noskov VN, Glass JI, Venter JC, Hutchison CA 3rd, Smith HO (2008) Complete chemical synthesis, assembly, and cloning of a Mycoplasma genitalium genome. *Science* **319**: 1215–1220.

Gillespie DT (1977) Exact stochastic simulation of coupled chemical-reactions. *J Phys Chem* **81**: 2340–61.

Goldstein JC, Waterhouse NJ, Juin P, Evan GI, Green DR (2000) The coordinate release of cytochrome c during apoptosis is rapid, complete and kinetically invariant. *Nat Cell Biol* **2**: 156–162.

Gossen M, Bujard H (1992) Tight control of gene expression in mammalian cells by tetracycline-responsive promoters. *Proc Natl Acad Sci USA* **89**: 5547–5551.

Gossen M, Freundlieb S, Bender G, Mller G, Hillen W, Bujard H (1995) Transcriptional activation by tetracyclines in mammalian cells. *Science* **268**: 1766–1769.

Greber D, Fussenegger M (2007) Mammalian synthetic biology: engineering of sophisticated gene networks. *J Biotechnol* **130**: 329–345.

Guido NJ, Wang X, Adalsteinsson D, McMillen D, Hasty J, Cantor CR, Elston TC, Collins JJ (2006) A bottom-up approach to gene regulation. *Nature* **439**: 856-860.

Hasty J, McMillen D, Collins JJ (2002) Engineered gene circuits. *Nature* **420**: 224–230.

Hasty J, Pradines J, Dolnik M, Collins JJ (2000) Noise-based switches and amplifiers for gene expression. *Proc Natl Acad Sci USA* **97**: 2075–2080.

Hersen P, McClean MN, Mahadevan L, Ramanathan S (2008) Signal processing by the HOG MAP kinase pathway. *Proc Natl Acad Sci USA* **105**: 7165–7170.

Hoffmann A, Levchenko A, Scott ML, Baltimore D (2002) The IkB-NF-kB signaling module: temporal control and selective gene activation. *Science* **298**: 1241–1245.

International Human Genome Sequencing Consortium (2001) Initial sequencing and analysis of the human genome. *Nature* **409**: 860–921.

International Human Genome Sequencing Consortium (2004) Finishing the euchromatic sequence of the human genome. *Nature* **431**: 931-945.

Irish JM, Kotecha N, Nolan GP (2006) Mapping normal and cancer cell signalling networks: towards single-cell proteomics. *Nat Rev Cancer* **6**: 146–155.

Kaern M, Elston TC, Blake WJ, Collins JJ (2005) Stochasticity in gene expression: from theories to phenotypes. *Nat Rev Genet* **6**: 451-464.

Kaiser J (2008) DNA sequencing. A plan to capture human diversity in 1000 genomes. *Science* **319**: 395.

Kearns JD, Basak S, Werner SL, Huang CS, Hoffmann A (2006) IκBϵ provides negative feedback to control NF-κB oscillations, signaling dynamics, and inflammatory gene expression. *J Cell Biol* **173**: 659–64.

Kim JR, Yoon Y, Cho KH (2008) Coupled feedback loops form dynamic motifs of cellular networks. *Biophys J* **94**: 359–365.

Kitano H (2002) Systems biology: a brief overview. *Science* **295**: 1662–1664.

Koenig R (2009) Genome scans: impatient for the payoff. *Science* **324**: 448.

Kramer BP, Fussenegger M (2005) Hysteresis in a synthetic mammalian gene network. *Proc Natl Acad Sci USA* **102**: 9517–9522.

Kramer BP, Viretta AU, Daoud-El-Baba M, Aubel D, Weber W, Fussenegger M (2004) An engineered epigenetic transgene switch in mammalian cells. *Nat Biotechnol* **22**: 867–870.

Krishna S, Jensen MH, Sneppen K (2006) Minimal model of spiky oscillations in NF-kappaB signaling. *Proc Natl Acad Sci USA* **103**: 10840–10845.

Kruse K, Pantazis P, Bollenbach T, Julicher F, Gonzalez-Gaitan M (2004) Dpp gradient formation by dynamin-dependent endocytosis: receptor trafficking and the diffusion model. *Development* **131**: 4843–4856.

Krutzik PO, Crane JM, Clutter MR, Nolan GP (2008) High-content single-cell drug screening with phosphospecific flow cytometry. *Nat Chem Biol* **4**: 132–142.

Lahav G, Rosenfeld N, Sigal A, Geva-Zatorsky N, Levine AJ, Elowitz MB, Alon U (2004) Dynamics of the p53-Mdm2 feedback loop in individual cells. *Nat Genet* **36**: 147–150.

Lai K, Robertson MJ, Schaffer DV (2004) The sonic hedgehog signaling system as a bistable genetic switch. *Biophys J* **86**: 2748–2757.

Lander AD, Nie Q, Wan FY (2002) Do morphogen gradients arise by diffusion? *Dev Cell* **2**: 785–796.

Legewie S, Bluthgen N, Herzel H (2006) Mathematical modeling identifies inhibitors of apoptosis as mediators of positive feedback and bistability. *PLoS Comput Biol* **2**: e120.

Lipniacki T, Paszek P, Brasier AR, Luxon BA, Kimmel M (2006) Stochastic regulation in early immune response. *Biophys J* **90**: 725–742.

Lipshtat A, Perets HB, Balaban NQ, Biham O (2005) Modeling of negative autoregulated genetic networks in single cells. *Gene* **347**: 265–271.

Longo D, Hasty J (2006) Dynamics of single-cell gene expression. *Mol Syst Biol* **2**: 64.

Ma L, Wagner J, Rice JJ, Hu W, Levine AJ, Stolovitzky GA (2005) A plausible model for the digital response of p53 to DNA damage. *Proc Natl Acad Sci USA* **102**: 14266–14271.

May T, Eccleston L, Herrmann S, Hauser H, Goncalves J, Wirth D (2008) *PLoS ONE* **3**: e2372.

McAdams HH, Arkin A (1999) Its a noisy business! genetic regulation at the nanomolar scale. *Trends Genet* **15**: 65-69.

Nelson DE, Ihekwaba AEC, Elliott M, Johnson JR, Gibney CA, Foreman BE, Nelson G, See V, Horton CA, Spiller DG, Edwards SW, McDowell HP, Unitt JF, Sullivan E, Grimley R, Benson N, Broomhead D, Kell DB, White MRH (2004) Oscillations in NF-κB signaling control the dynamics of gene expression. *Science* **306**: 704–708.

Newman JR, Ghaemmaghami S, Ihmels J, Breslow DK, Noble M, Derisi JL, Weissman JS (2006) Single-cell proteomic analysis of S. cerevisiae reveals the architecture of biological noise. *Nature* **441**: 840-846.

Ozbudak EM, Thattai M, Kurtser I, Grossman AD, van Oudenaarden A (2002) Regulation of noise in the expression of a single gene. *Nat Genet* **31**: 69-73.

Pedraza JM, van Oudenaarden A (2005) Noise propagation in gene networks. *Science* **307**: 1965-1969.

Raj A, Peskin CS, Tranchina D, Vargas DY, Tyagi S (2006) Stochastic mRNA synthesis in mammalian cells. *PLoS Biol* **4**: e309.

Raj A, van Oudenaarden A (2008) Nature, nurture, or chance: stochastic gene expression and its consequences. *Cell* **135**: 216–226.

Ramsey S, Ozinsky A, Clark A, Smith KD, de Atauri P, Thorsson V, Orrell D, Bolouri H (2006) Transcriptional noise and cellular heterogeneity in mammalian macrophages. *Philos Trans R Soc London B Biol Sci* **361**: 495-506.

Ramsey SA, Smith JJ, Orrell D, Marelli M, Petersen TW, de Atauri P, Bolouri H, Aitchison JD (2006) Dual feedback loops in the GAL regulon suppress cellular heterogeneity in yeast. *Nat Genet* **38**: 1082–1087.

Rao CV,Wolf DM, Arkin AP (2002) Control, exploitation and tolerance of intracellular noise. *Nature* **420**: 231-237.

Raser JM, O'Shea EK (2004) Control of stochasticity in eukaryotic gene expression. *Science* **304**: 1811–1814.

Raser JM, O'Shea EK (2005) Noise in gene expression: origins, consequences, and control. *Science* **309**: 2010–2013.

Rehm M, Dussmann H, Janicke RU, Tavare JM, Kogel D, Prehn JH (2002) Single-cell fluorescence resonance energy transfer analysis demonstrates that caspase activation during apoptosis is a rapid process. *J Biol Chem* **277**: 24506–24514.

Ren B, Robert F, Wyrick JJ, Aparicio O, Jennings EG, Simon I, Zeitlinger J, Schreiber J, Hannett N, Kanin E, Volkert TL, Wilson CJ, Bell SP, Young RA (2000) Genome-wide location and function of DNA binding proteins. *Science 290*: 2306–2309.

Rennel E, Gerwins P (2002) How to make tetracycline-regulated transgene expression go on and off. *Anal Biochem* **309**: 79–84.

Rosenfeld N, Elowitz MB, Alon U (2002) Negative autoregulation speeds the response times of transcription networks. *J Mol Biol* **323**: 785-793.

Rosenfeld N, Young JW, Alon U, Swain PS, Elowitz MB (2005) Gene regulation at the single-cell level. *Science* **307**: 1962–1965.

Rossi FM, Guicherit OM, Spicher A, Kringstein AM, Fatyol K, Blakely BT, Blau HM (1998) Tetracycline-regulatable factors with distinct dimerization domains allow reversible growth inhibition by p16. *Nat Genet* **20**: 389–393.

Savageau MA (1974) Comparison of classical and autogenous systems of regulation in inducible operons. *Nature* **252**: 546-549.

Shimojo H, Ohtsuka T, Kageyama R (2008) Oscillations in notch signaling regulate maintenance of neural progenitors. *Neuron* **58**: 52–64.

Sigal A, Milo R, Cohen A, Geva-Zatorsky N, Klein Y, Alaluf I, Swerdlin N, Perzov N, Danon T, Liron Y, Raveh T, Carpenter AE, Lahav G, Alon U (2006) Dynamic proteomics in individual human cells uncovers widespread cell-cycle dependence of nuclear proteins. *Nat Methods* **3**: 525-531.

Skotheim JM, Di Talia S, Siggia ED, Cross FR (2008) Positive feedback of G1 cyclins ensures coherent cell cycle entry. *Nature* **454**: 291–296.

Sprinzak D, Elowitz MB (2005) Reconstruction of genetic circuits. *Nature* **438**: 443–448.

Stricker J, Cookson S, Bennett MR, Mather WH, Tsimring LS, Hasty J (2008) A fast, robust and tunable synthetic gene oscillator. *Nature* **456**: 516–519.

Swain PS, Elowitz MB, Siggia ED (2002) Intrinsic and extrinsic contributions to stochasticity in gene expression. *Proc Natl Acad Sci USA* **99**: 12795–12800.

Tannu NS, Hemby SE (2006) Two-dimensional fluorescence difference gel electrophoresis for comparative proteomics profiling. *Nat Protoc* **1**: 1732–1742.

Tergaonkar V (2006) NFkappaB pathway: a good signaling paradigm and therapeutic target. *Int J Biochem Cell Biol* **38**: 1647–1653.

Thattai M, van Oudenaarden A (2001) Intrinsic noise in gene regulatory networks. *Proc Natl Acad Sci USA* **98**: 8614–8619.

Tyson JJ, Chen KC, Novak B (2003) Sniffers, buzzers, toggles and blinkers: dynamics of regulatory and signaling pathways in the cell. *Curr Opin Cell Biol* **15**: 221–231.

Uetz P (2002) Two-hybrid arrays. *Curr Opin Chem Biol* **6**: 57–62.

Venter JC, Adams MD, Myers EW, Li PW, Mural RJ, Sutton GG, Smith HO, Yandell M, Evans CA, Holt RA, Gocayne JD, Amanatides P, Ballew RM, Huson DH, Wortman JR, Zhang Q, Kodira CD, Zheng XH, Chen L, Skupski M, Subramanian G, Thomas PD, Zhang J, Gabor Miklos GL, Nelson C, Broder S, Clark AG, Nadeau J, McKusick VA, Zinder N, Levine AJ, Roberts RJ, Simon M, Slayman C, Hunkapiller M, Bolanos R, Delcher A, Dew I, Fasulo D, Flanigan M, Florea L, Halpern A, Hannenhalli S, Kravitz S, Levy S, Mobarry C, Reinert K, Remington K, Abu-Threideh J, Beasley E, Biddick K, Bonazzi V, Brandon R, Cargill M, Chandramouliswaran I, Charlab R, Chaturvedi K, Deng Z, Di Francesco V, Dunn P, Eilbeck K, Evangelista C, Gabrielian AE, Gan W, Ge W, Gong F, Gu Z, Guan P, Heiman TJ, Higgins ME, Ji RR, Ke Z, Ketchum KA, Lai Z, Lei Y, Li Z, Li J, Liang Y, Lin X, Lu F, Merkulov GV, Milshina N, Moore HM, Naik AK, Narayan VA, Neelam B, Nusskern D, Rusch DB, Salzberg S, Shao W, Shue B, Sun J, Wang Z, Wang A, Wang X, Wang J, Wei M, Wides R, Xiao C, Yan C, Yao A, Ye J, Zhan M, Zhang W, Zhang H, Zhao Q, Zheng L, Zhong F, Zhong W, Zhu S, Zhao S, Gilbert D, Baumhueter S, Spier G, Carter C, Cravchik A, Woodage T, Ali F, An H, Awe A, Baldwin D, Baden H, Barnstead M, Barrow I, Beeson K, Busam D, Carver A, Center A, Cheng ML, Curry L, Danaher S, Davenport L, Desilets R, Dietz S, Dodson K, Doup L, Ferriera S, Garg N, Gluecksmann A, Hart B, Haynes J, Haynes C, Heiner C, Hladun S, Hostin D, Houck J, Howland T, Ibegwam C, Johnson J, Kalush F, Kline L, Koduru S, Love A, Mann F, May D, McCawley S, McIntosh T, McMullen I, Moy M, Moy L, Murphy B, Nelson K, Pfannkoch C, Pratts E, Puri V, Qureshi H, Reardon M, Rodriguez R, Rogers YH, Romblad D, Ruhfel B, Scott R, Sitter C, Smallwood M, Stewart E, Strong R, Suh E, Thomas R, Tint NN, Tse S, Vech C, Wang G, Wetter J, Williams S, Williams M, Windsor S, Winn-Deen E, Wolfe K, Zaveri J, Zaveri K, Abril JF, Guig R, Campbell MJ, Sjolander KV, Karlak B, Kejariwal A, Mi H, Lazareva B, Hatton T, Narechania A, Diemer K, Muruganujan A, Guo N, Sato S, Bafna V, Istrail S, Lippert R, Schwartz R, Walenz B, Yooseph S, Allen D, Basu A, Baxendale J, Blick L, Caminha M, Carnes-Stine J, Caulk P, Chiang YH, Coyne M, Dahlke C, Mays A, Dombroski M, Donnelly M, Ely D, Esparham S, Fosler C, Gire H, Glanowski S, Glasser K, Glodek A, Gorokhov M, Graham K, Gropman B, Harris M, Heil J, Henderson S, Hoover J, Jennings D, Jordan C, Jordan J, Kasha J, Kagan L, Kraft C, Levitsky A, Lewis M, Liu X, Lopez J, Ma D, Majoros W, McDaniel J, Murphy S, Newman M, Nguyen T, Nguyen N, Nodell M, Pan S, Peck J, Peterson M, Rowe W, Sanders R, Scott J, Simpson M, Smith T, Sprague A, Stockwell T, Turner R, Venter E, Wang M, Wen M, Wu D, Wu M, Xia A, Zandieh A, Zhu X (2001) The sequence of

the human genome. *Science* **291**: 1304–1351.

Vogelstein B, Lane D, Levine AJ (2000) Surfing the p53 network. *Nature* **408**: 307–310.

Volfson D, Marciniak J, Ostroff N, Blake W, Tsimring LS, Hasty J (2006) Origins of extrinsic variability in eukaryotic gene expression. *Nature* **439**: 861–864.

Weber W, Fussenegger M (2009). Engineering of synthetic mammalian gene networks. *Chem Biol* **16**: 287–297.

Weber W, Kramer BP, Fussenegger M (2007) A genetic time-delay circuitry in mammalian cells. *Biotechnol Bioeng* **98**: 894–902.

Yao G, Lee TJ, Mori S, Nevins JR, You L (2008) A bistable Rb-E2F switch underlies the restriction point. *Nat Cell Biol* **10**: 476–482.